Polygonal peatlands and treed peat plateau in Northwest Hudson Bay Lowlands, Canada: Holocene development and permafrost dynamics

Tiina H. M. Kolari[a,1], Laure Gandois[b], Frédéric Bouchard[c,d,e], Alison E. Cassidy[f], Nicole K. Sanderson[a,g], Rémi Tremouille[b], Julien Arsenault[c,e,h], Maialen Barret[b], Adam Collingwood[f], Lucile Cosyn Wexsteen[c,d,e], Sylvain Ferrant[i], LeeAnn Fishback[j], Karen Richardson[f], & Michelle Garneau[a,g]

This is the revised version of the manuscript submitted for peer-review *in Quaternary Science Reviews*. This version has slightly different content than the first version. Please note that, despite having undergone peer-review, the manuscript has not been accepted for publication. If accepted, the final version of this manuscript will be available via the *'Peer-reviewed publication DOI'* link on this webpage. (24.8.2026)

[a]Research Centre in Earth System Dynamics (GEOTOP), Université du Québec à Montréal, Montréal, QC, Canada

[b]Centre de Recherche sur la Biodiversité et l'Environnement (CRBE), Université de Toulouse, CNRS-UPS-INPT, Toulouse, France

[c]Department of Applied Geomatics & Centre d'applications et de recherche en télédétection (CARTEL), Université de Sherbrooke, Sherbrooke, QC, Canada

[d]Centre d'études nordiques (CEN), Québec, QC, Canada

[e]Groupe de recherche interuniversitaire en limnologie (GRIL), Université de Montréal, Montréal, QC, Canada

[f]Parks Canada, Gatineau, QC, Canada

[g]Département de Géographie, Université du Québec à Montréal, Montréal, QC, Canada

[h]Département des sciences biologiques, Université du Québec à Montréal, Montréal, QC, Canada

[i]Centre d'Etudes Spatiales de la Biosphère (CESBIO), Université de Toulouse, CNES/CNRS/INRAE/IRD/UT3, Toulouse, France

[j]Parks Canada, Churchill, MB, Canada

Corresponding author:

Tiina H. M. Kolari

Email: tiina.kolari@uef.fi

Phone number: +35840 543 9545

[1]Present address: Department of Environmental and Biological Sciences, University of Eastern Finland, Joensuu Campus, Yliopistokatu 7, P. O. Box 111, FI-80101 Joensuu, Finland

Abstract

Since the retreat of the Laurentide Ice Sheet, peatland development in the Hudson Bay Lowlands (HBL) has been mainly influenced by postglacial isostatic rebound and climate. We studied the timing of permafrost aggradation and the successional trajectories of low Arctic and subarctic polygonal peatlands and a northern boreal treed peat plateau in Wapusk National Park (WNP) in northwestern HBL. We also explored the timing of peatland initiation and long-term carbon accumulation between peatland types. Peatland initiation in WNP dates to at least 6000 cal BP, and peat thickness and carbon mass were higher in treed peat plateaus (mean: 71.7±21.4 (SE) kg C m^{-2}) and intermediate-centred polygonal peatlands (63.2±7.14 (SE) kg C m^{-2}) than in non-permafrost fens (20.4 ±1.75 (SE) kg C m^{-2}). In the subarctic and northern boreal forest zones, permafrost peatlands were preceded by treed *Sphagnum* bogs with *Picea mariana* and *P. glauca*. Abrupt declines in peat and carbon accumulation in subarctic sites ~1500–1050 cal BP reflected cooling from the Dark Ages Cold Period to the Little Ice Age (LIA). Low peat accumulation, spruce disappearance ~1330–780 cal BP, and the shift toward vegetation dominated by *Dicranum* spp. mosses and *Cladonia* lichens suggest that permafrost aggradation occurred across the study region during the LIA. These results further suggest that in the subarctic tundra, polygons formed in *Sphagnum*-dominated peat plateaus, rather than evolving from low-centered polygons. The low Arctic polygon was characterized by wet fen vegetation until permafrost developed ~190 cal BP, but the exact successional pathway remains uncertain.

Keywords: age-depth modelling, carbon accumulation, Dark Ages Cold Period, Little Ice Age, permafrost aggradation, plant macrofossils, polygon formation

Highlights

- Permafrost developed during the Little Ice Age
- Carbon stocks higher in permafrost peat plateaus than in non-permafrost fens
- Development history differed between low Arctic and subarctic peatlands
- In subarctic tundra, treed *Sphagnum* bogs preceded permafrost peatlands
- Wet fen preceded the low Arctic polygonal peatland

1. Introduction

Northern peatlands store 415 ± 150 Pg of carbon (C), of which approximately half is found in permafrost regions (Hugelius et al., 2020). Currently, the Arctic is warming almost four times faster than the rest of the globe (Rantanen et al., 2022), resulting in frozen ground temperatures and active layer thicknesses increasing across the Arctic (Biskaborn et al., 2019; Langer et al., 2024; Smith et al., 2022), and posing a threat to the C stored in permafrost (Hugelius et al., 2020; Schuur et al., 2015, 2022; Treat et al., 2021). Many continuous permafrost regions are characterized by ice-wedge polygon peatlands, where permafrost thaw can cause variable changes in peatland microtopography, hydrology, and vegetation (Jorgenson et al., 2006; 2022; Parmentier et al., 2014; Wolter et al., 2016, 2018). These changes range from the collapse of large ice wedges and the formation of thermokarst ponds with an increase in aquatic vegetation (Jorgenson et al., 2006, 2022) to lake desiccation (Bouchard et al., 2013; Webb et al., 2022) and the creation of dry elevated polygon centres with increasing cover of lichens and shrubs (Liljedahl et al., 2016; Wolter et al., 2016, 2018).

To better understand these landscape-level changes and predict future responses to ongoing warming, it is important to consider how polygonal peatlands typically form, and how that connects to permafrost aggradation and degradation. It is known that ice-wedge polygons form through thermal contraction cracking of frozen peat or mineral soil in high-latitude areas, creating a network of either low-, intermediate-, or high-centred ice-wedge polygons (Mackay, 2000; Fortier & Allard, 2005). In terms of vegetation, low-centred polygons are typically dominated by fen vegetation (sedges and mosses of wet habitats), while lichens and dwarf shrubs are abundant on the dry surfaces of intermediate- and high-centred polygons (Mackay, 2000; Wolter et al., 2016). Low-centred polygons often form on newly exposed mineral soil in coastal lowlands or drained lakes and can evolve into intermediate-centred polygons through peat accumulation in the shallow polygons/pools (Mackay, 2000) or through ice wedge degradation (Liljedahl et al., 2016). Eventually, intermediate-centred polygons can develop rapidly into high-centred polygons through further ice-wedge degradation and deepening of water-filled troughs surrounding the polygons (Abolt et al., 2020; Kanevskiy et al., 2017; Liljedahl et al., 2016; Wolter et al., 2018). However, the exact pathways can depend on local hydrology, climate, and vegetation (De Klerk et al., 2011; Ellis et al., 2008; Parmentier et al., 2024; Payette et al., 1986; Wolter et al., 2018).

Polygon-forming processes are particularly important in northwestern regions of the Hudson Bay Lowlands (HBL). The entire HBL peatland complex is the second largest in the world, with an estimated C storage of ~30 Pg (Li et al., 2025). The Holocene development of permafrost peatlands in the northern HBL has been previously studied by Dredge & Mott (2003) and Kuhry (2008). These studies mainly focused on treed/forested peat plateaus in the boreal forest along the Hudson Bay railroad south of Churchill (Manitoba), where peatland initiation followed paludification of upland forests (Kuhry 2008), and the oldest basal ages of peatlands date to between 7100 and 6800 cal BP (Dredge & Mott 2008; Kuhry 2008). Using pollen analysis, Dredge & Mott (2003) concluded that vegetation has been relatively stable over the past six millennia, characterized by *Sphagnum fuscum* and *Picea mariana*. However, little is known about the development of polygonal peatlands in this region.

Currently, the extensive polygonal peatlands in the northwestern HBL are mostly lichen-dominated and intermediate-centred. It remains unclear whether these dry polygons have formed rapidly from wet polygons during the past century or decades, in response to ongoing warming and ice-wedge degradation, as reported from the Low and High Arctic regions (Abolt et al., 2020; Kanevskiy et al., 2017; Liljedahl et al., 2016; Wolter et al., 2018), or whether their formation is climate-driven by long-term (centennial- to millennial-scale) dynamics. For example, some evidence exists that in subarctic regions, ice-wedges and dry polygons could also form in relatively dry conditions after natural tree removal (Payette et al., 1986), instead of evolving from wet, low-centred polygons. A comprehensive understanding of the Holocene history of the polygonal peatlands in the northwestern HBL is crucial, particularly to accurately estimate the fate of vast C storage under warming and increased microbial activity (Kirkwood et al., 2021; Schuur et al., 2015, 2022; Treat et al., 2021).

In this study, we explore Holocene peatland development and permafrost dynamics in the northwestern Hudson Bay Lowlands. Specifically, our research questions were: 1) How did the successional trajectory differ between vegetation zones (low Arctic tundra, subarctic tundra, and northern boreal forest), 2) when did permafrost aggradation occur, and 3) did permafrost conditions remain stable throughout the Holocene? To answer these questions, we collected peat profiles for paleoecological reconstructions from four dry, intermediate-centred polygonal peatlands and one treed peat plateau. In addition to detailed plant macrofossil analysis of the five profiles, we estimated the timing of peatland initiation and permafrost aggradation, as well as long-term peat and carbon accumulation rates across the different vegetation zones in the region based on radiocarbon dating and geochemical data.

2 Materials and Methods

2.1 Study area and sites

This study was conducted in Wapusk National Park (WNP) and the Churchill Wildlife Management Area, located along the western coast of Hudson Bay, near Churchill (58° 46' 09" N, 94° 10' 09" W) in northern Manitoba, Canada (**Figure 1**). WNP covers 11 475 km^2. The region was covered by the Laurentide Ice Sheet until ~8.5 ka BP, and the postglacial Tyrrell Sea transgressed over the area by ~8.1 ka BP (Gauthier et al., 2020; Dalton et al., 2023). Since then, peatland development has been largely driven by glacial isostatic adjustment and land emergence from the sea (Dredge & Mott, 2003; Glaser et al., 2004; Packalen et al., 2014), with a present-day uplift rate of ~10 mm a^{-1} (Sella et al., 2007).

The study area is located within both continuous and discontinuous permafrost (Obu et al., 2019; **Figure 1a**). In 1991–2020, mean annual air temperature (MAAT) in Churchill was −6.0 °C, and mean annual precipitation (MAP) was 448 mm (Environment and Climate Change Canada, *open data)*. The mean daily temperature of the coldest month (January) was −25.3 °C, and that of the warmest month (July) was 13.0 °C. WNP spans over three vegetation zones from southwest to northeast: northern boreal woodland, subarctic woodland-tundra, and low Arctic shrub tundra (Baldwin et al., 2020; **Figure 1b**). Hereafter, we refer to these zones as northern boreal forest, subarctic tundra, and low Arctic tundra, respectively.

A total of 21 peat profiles were collected from 20 sites between 2023 and 2025 (**Figure 1b**; **Supplemental Table S1**). Peat coring locations were preliminarily selected based on satellite imagery, the Wapusk ecotype map report (Pomonorenko et al., 2014), and helicopter aerial surveys. The aim was to cover all types of permafrost and non-permafrost peatlands described by Pomonorenko et al. (2014). Moreover, an effort was made to sample near one pond/lake in each vegetation zone, as included in the ecological integrity monitoring program for Wapusk National Park (lakes WAP05 in low Arctic tundra, WAP34 in subarctic tundra, and WAP27 in northern boreal forest).

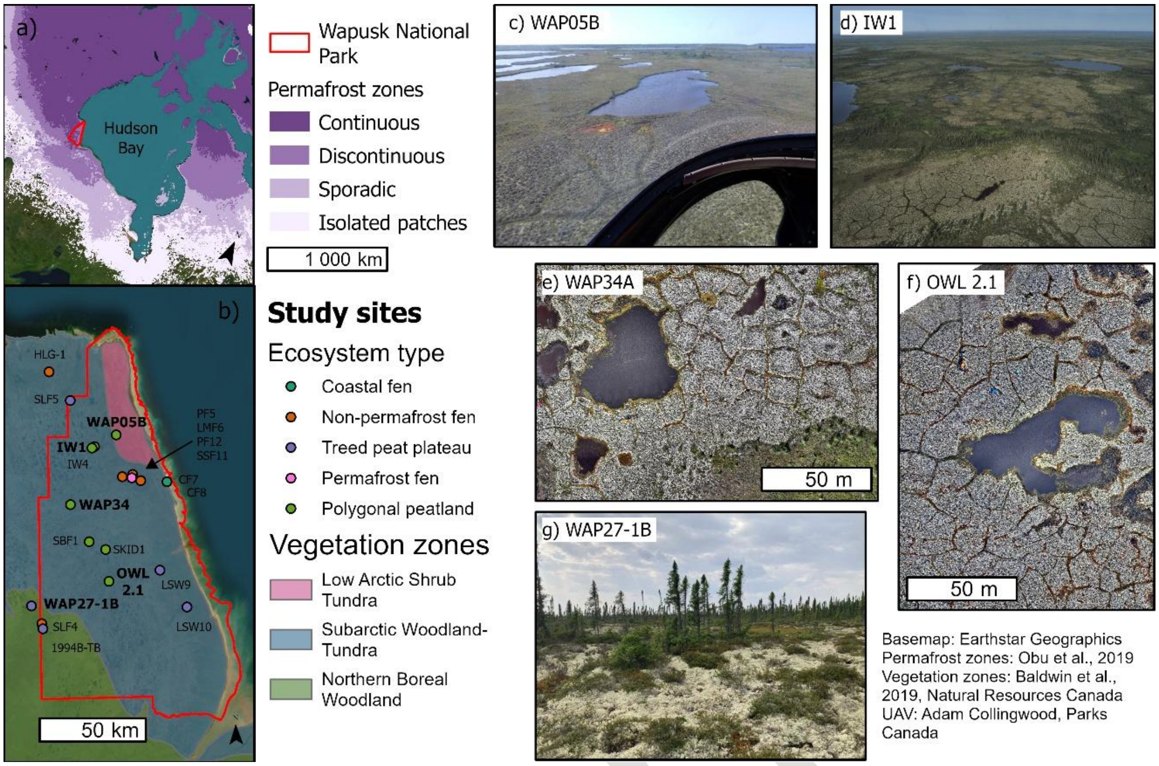

Figure 1. *Study area and peat coring locations. Location of Wapusk National Park (WNP) in northwestern Hudson Bay Lowlands (a) and peat coring locations in WNP and Churchill Wildlife Management Area, across Low Arctic Shrub Tundra, Subarctic Woodland-Tundra, and Northern Boreal Woodland zones (b). Photos and UAV images are presented for paleoreconstruction sites: low Arctic polygonal peatland WAP05B (c), subarctic polygonal peatlands IW1 (d), WAP34A (e), OWL 2.1 (f), and a treed peat plateau WAP27-1B (g). At the WAP34 site, peat cores were collected from both the polygon centre and ice-wedge trough. The map contains information licensed under the Open Government Licence – Canada.*

2.1.1 Sites for paleoecological reconstructions

Peat profiles for detailed paleoecological reconstructions were collected from four polygon centres (WAP05B, WAP34A, OWL 2.1, and IW1) and one treed peat plateau (WAP27-1B), representing the three vegetation zones (**Figure 1**). At the WAP34 site, a peat core was also collected from an ice-wedge trough (WAP34B) for radiocarbon (^{14}C) dating (see section 2.4).

Most polygons in this region are intermediate-centred, and they are characterized by the dominance of *Cladonia* lichens, particularly *C. arbuscula, C. rangiferina*, and *C. stellaris*. Although some ice-wedge degradation was observed, it is noteworthy that most ice-wedge troughs were only slightly lower than polygon centres, and that they were not water-filled. Instead, hummock-level *Sphagnum* moss species (mainly *S. fuscum*) were abundant in the troughs. Of dwarf shrubs, *Empetrum nigrum* and *Rhododendron tomentosum* were common both on polygon centres and troughs, particularly at the WAP05 site. Treed peat plateaus were dominated by *C. stellaris, Picea glauca*, and *P. mariana*.

The active layer thickness (ALT) was 50 cm at the treed plateau (WAP27-1B), 56 cm at the ice-wedge trough (WAP34B) and ranged from 32 to 45 cm in polygon centres. The measurements were taken either in mid-July 2024 or mid-August 2023, while the maximum ALT is reached in late August or September.

2.1.2 Sites for estimating peatland initiation and carbon accumulation across the region

To estimate the timing of peatland initiation, total carbon masses, and long-term apparent rates of carbon accumulation (LORCA) across the study region, we collected 15 additional peat profiles **(Figure 1; Table S1)**, spanning from the subarctic coastal fens to the boreal forest and corresponding to all permafrost and non-permafrost peatland types described by Pomonorenko et al. (2014), except for *Sphagnum* poor fens. Permafrost sites comprised three polygonal peatlands, four treed/forested peat plateaus, and one open rich fen. Non-permafrost sites comprised two treed rich fens, four open rich fens, and one open poor fen.

2.2 Field sampling

Fieldwork was mainly conducted during the 2023–2025 growing seasons, with two peat profiles collected in March 2025 (**Table S1**). At permafrost sites, the peat from the active layer was collected into metal boxes (30 × 12 × 6 cm or 50 × 12 × 6 cm). Beneath the active layer, frozen cores were retrieved using a SIPRE permafrost corer outfitted with a 7.62 cm core barrel. In non-permafrost fens, peat cores were only collected in metal boxes, as the peat thickness did not exceed 51 cm over mineral soil. Permafrost cores were kept at −20 °C and non-permafrost cores at 4 °C until analyses.

2.3 Laboratory analyses

2.3.1 Bulk density, total organic carbon content, and C/N ratio

All peat cores were sliced into 1-cm sections using a serrated knife. Permafrost cores were cut after thawing at 4 °C for 3-7 days or at room temperature overnight, preferably when they were still icy but easy to slice. No permafrost cores had segregated ice lenses (**Supplemental Figures S1-S5**), and the length of each core was measured frozen and after thawing, to estimate potential water loss and compression. On average, the difference between frozen and thawed length was 1 cm (0-2.5 cm). This compression was considered to have a limited effect on subsequent analyses. Measurements of core length taken while the peat cores were frozen were used in all analyses, including age–depth modelling and calculations of peat and carbon accumulation rates.

The total organic matter content was analyzed using the loss-on-ignition method (LOI; Chambers et al., 2011), with contiguous 1-cm intervals for paleoreconstruction sites and contiguous 3-cm sections for other sites. For each 1- or 3-cm layer, a 3 cm^3 peat sample was weighed and dried at 105 °C overnight to determine the dry bulk density (g cm^{-3}). The dried samples were burned at 550 °C for three hours to determine organic matter content (%) and to calculate organic matter density (g cm^{-3}). Organic C density (g cm^{-3}) was calculated by multiplying the total organic matter density by 0.5 (Turunen et al., 2002). Total C mass (g cm^{-2}) for each site was obtained by summing the organic C density values of all 1-cm peat layers, then converted to kg C m^{-2}. In cases when peat cores were analyzed for LOI in 3-cm layers, organic C densities were first multiplied by the peat layer thickness. Total C mass (g C m^{-2}) was also calculated for each zone identified in plant macrofossil profiles (see *section 2.3.2*).

For WAP27-1B and OWL 2.1 cores, total carbon and nitrogen (N) contents (%) were analyzed at 2-cm intervals to calculate the C/N ratio. Prior to analysis, peat samples of ca. 2 cm^3 were dried at 60 °C for approximately 48 hours and then ground using a mortar and pestle. Subsequently, subsamples of 1.5–2.2 mg of dried peat were analyzed for C and N using an Elementar Vario MicroCube analyzer at the light stable isotope geochemistry laboratory at Geotop-UQAM in Montreal, Canada. For WAP05B and WAP34A, C and N contents (%) were analyzed from paired profiles collected on the same day, less than 1 m apart. The paired profiles were analyzed in 5-cm sections at the PAPC (CRBE laboratory, Toulouse, France) on 15 to 20 mg subsamples, using an elemental analyzer ThermoScientific, Flash 2000, and NCS FC and Soil CNS Reference as certified materials. IW1 was not analyzed for C and N contents because analytical resources were prioritized for two high-resolution peat cores and no paired core with complementary data was available.

2.3.2 Plant macrofossils

Peat profiles for paleoecological reconstructions were analyzed for plant macrofossil composition at 4 cm intervals. Macrofossil composition was determined from 3 cm^3 peat samples, which were pre-treated following the protocol of Mauquoy et al. (2010), with some minor adjustments. Peat samples were first gently boiled in a 5% KOH solution for 5-10 minutes, then rinsed with distilled water and sieved through a 125 μm sieve. The abundance of plant macrofossil groups (*Sphagnum* mosses, brown mosses, herbaceous, ligneous, and lichens) was estimated in percentages using a stereoscopic microscope. Coniferous needles, ericaceous leaves, Cyperaceae seeds and rhizomes, charcoal fragments, Chironomidae head capsules, *Daphnia* resting eggs (ephippia), and Oribatid mites were counted. When possible, brown mosses were identified to the species level, following Faubert (2014). *Sphagnum* mosses were identified to section, aggregate, or species level by checking 50 random *Sphagnum* branch leaves with a light microscope, following Laine et al. (2009) and Ayoutte & Rochefort (2019). Leaf counts were converted to percentages, with one leaf representing 2% of the total abundance of *Sphagnum* mosses. They were identified to species level only when stem leaves were also present. Nomenclature of all species follows Global Biodiversity Information Facility (www.gbif.org, accessed November 20th, 2025).

Plant macrofossil diagrams were created using the *riojaPlo*t package (Juggins, 2025) in R version 4.5.1 (R Core Team, 2025). Taxa that reached at least 5 or 6% in abundance or countable macrofossils that appeared at least three or five times (depending on the core) were included in the diagrams. Different zones in peat profiles were identified using constrained incremental sum of squares hierarchical clustering (CONISS) and the function chclust in the *rioja* package (Juggins, 2024). CONISS was performed with surface lichens, except for WAP05B, where dwarf shrubs dominate contemporary vegetation. Surface vegetation is not commonly included in macrofossil diagrams, and lichens tend to decompose rapidly (Harris et al., 2018). Still, in our opinion, it is crucial to recognize the contemporary lichen-dominated phase from the preceding one in the profiles.

2.4 ^{14}C dating and chronologies

A total of 43 samples were submitted to the A.E. Lalonde AMS Laboratory (University of Ottawa, Canada) for radiocarbon (^{14}C) dating. The basal age of each core and the major transitions in plant macrofossil assemblages or bulk density were dated for paleoreconstructions. *Sphagnum* moss stems were preferably selected for dating. Ericaceous leaves, coniferous needles, moss stems, and Cyperaceae seeds were selected when *Sphagnum* stems were not sufficiently abundant. Two charcoal samples were submitted to date wildfires at the WAP27-1B site. Bulk peat samples or wood fragments were selected when the basal peat was highly decomposed or comprised mainly of Cyperaceae tissue and rootlets. Radiocarbon dates were calibrated using OxCal v4.4 (Bronk Ramsey, 2009) and the IntCal20 calibration curve (Reimer et al., 2020) and are presented in calibrated years before present (cal BP, where BP is 1950 CE).

Bayesian age-depth modeling was performed for paleoreconstructions using the R package *rbacon* version 3.5.2 (Blaauw & Christen, 2011) in R version 4.5.1 (R Core Team, 2025) and the IntCal20 calibration curve (Reimer et al., 2020). The surface of the peat cores was set at -73 or -74 cal BP, corresponding to 2023 and 2024 when the cores were collected. Detailed AMS radiocarbon dating results for paleoreconstruction sites and age-depth models are available as supplementary material (**Table S2** and **Figures S6-S10**).

2.5 Peat and carbon accumulation rates

Peat accumulation rate (PAR; mm a^{-1}) and long-term apparent rate of carbon accumulation (LORCA, g C m^{-2} a^{-1}) were calculated for all 20 sites (excluding the WAP34B ice wedge trough) by dividing the peat thickness and total carbon mass by the basal calibrated median age. As point age estimates don't represent the uncertainties involved in ^{14}C dating (Millard, 2014), PAR and LORCA ranges calculated using the entire age probability ranges are presented for each site in **Supplementary Table S3**.

For the paleoreconstruction peat profiles, PAR and carbon accumulation rates (CAR; g C m^{-2} a^{-1}) were also calculated for each 1-cm peat layer and for each zone. First, the duration of each 1-cm peat layer and zone was determined as the difference between the median ages (cal BP) at their upper and lower boundaries, as estimated by the Bacon age–depth models.

Then, PAR was calculated for each 1-cm peat layer and zone by dividing the peat layer thickness by the time it represented, and CAR was calculated by dividing the C mass of the layer by the same time.

95% confidence intervals for the start and end of each zone, as well as PAR and CAR ranges for all zones, are found in **Table S4.** For clarity, the midpoints between the median ages of the start and end of successive zones were calculated, rounded to the nearest 10 years, and are used hereafter to define age intervals of different periods.

3 Results

3.1 Peatland initiation across WNP

In the northern boreal forest, peat accumulation began during the Mid-Holocene. The deepest and oldest peat deposit (2.6 m) was found at the treed plateau 1994B-TB (**Figure 1**), where peat started to accumulate approximately 6000 cal BP (**Table 1**). At the nearby treed plateau WAP27-1B, peat accumulation began ~5710 cal BP, whereas the basal age of the treed fen SLF4 was ~2600 cal BP.

At the polygonal peatlands in the subarctic tundra (WAP34A, OWL 2.1, IW1, IW4, and SBF1), peat accumulation began during the Late Holocene, ~3710–3220 cal BP. The polygonal peatland WAP05B had a younger basal age of 2390 cal BP, which is consistent with its location closer to the coast in the low Arctic tundra zone. Site SKID1 is a polygonal peatland located in the subarctic tundra, but close to Skidmore Lake, where peat accumulation started even later, roughly 1460 cal BP. The basal ages of subarctic treed and forested peat plateaus (LSW9, LSW10, and SLF5) ranged from ~1730 to 410 cal BP, with the youngest site (LSW10) found the closest to the coast. At subarctic non-permafrost fens (SSF11, PF12, LMF6, and HLG-1), peat accumulation began ~2160–1200 cal BP. Permafrost was found at one subarctic fen (PF5), where the basal age was ~2050 cal BP. The basal ages of subarctic coastal fens (CF7 and CF8) were each ~150 cal BP. However, the wide age range of coastal fens (~30–260 cal BP (1690–1920 CE)) reflects the reduced chronological precision due to the Suess effect and complexities in radiocarbon calibration (Reimer et al., 2020).

3.2 Long-term peat and carbon accumulation across WNP

In permafrost peatlands, the highest peat and carbon accumulation rates were found in treed/forested peat plateaus (**Table 1**), with a mean PAR of 0.73±0.23 (SE) mm a^{-1}, a mean carbon mass of 71.7±21.4 (SE) kg C m^{-2}, and a mean LORCA of 37.8±13.0 (SE) g C m^{-2} a^{-1}. LORCA ranged from 20.6 to 36.9 g C m^{-2} a^{-1}, except for LSW10, with LORCA of 88.4 g C m^{-2} a^{-1}. It is noteworthy, however, that the LSW10 site was the youngest of the peat plateaus, with a basal age of ~405 cal BP. In polygonal peatlands (n = 7), mean PAR was 0.41±0.04 mm a^{-1}, mean carbon mass 63.2±7.14 kg m^{-2}, and mean LORCA 22.0±3.03 g C m^{-2} a^{-1}. In non-permafrost fens (n = 5), mean PAR was 0.26±0.05 mm a^{-1}, mean carbon mass 20.4 ±1.75 kg m^{-2}, and mean LORCA 12.7 (SE ±1.64) g C m^{-2} a^{-1}. The subarctic coastal fens, CF7 and CF8, had the highest LORCA values of 71.9 and 113.3 g C m^{-2} a^{-1}, respectively, reflecting their young age (~260–30 cal BP) and incompletely decomposed peat. Also, the wide age range for CF7 and CF8 increases the uncertainty in both PAR and LORCA (**Table S3**).

3.3 Peat C and N content (%) and C/N ratio

Across four permafrost peat cores (WAP05B, WAP34A, OWL 2.1, and WAP27-1B), the median C content was 43.5% (IQR 42.2–44.7%), the median N content was 0.96% (IQR 0.62–2.0%), and the median C/N ratio was 45.3 (IQR 20.2–68.2). N content declined, and the C/N ratio increased with the shift from fen to bog vegetation dominated by *Dicranum* (**Figure 2**) or *Sphagnum* mosses. (**Figures 4-6**). Across sites, the highest median %N was found at WAP05B (2.24%) and the lowest at WAP34A (0.77%).

Median C contents did not differ between active layer and permafrost peat (43.3% and 43.6%, respectively), but median N content was lower in active layer peat (0.74%, IQR 0.43–1.10%) than in permafrost peat (1.02%, IQR 0.68–2.11%). Correspondingly, the median C/N ratio was higher in active layer peat (58.7, IQR 40.4–92.0) than in permafrost peat (43.5, IQR 18.9–63.5).

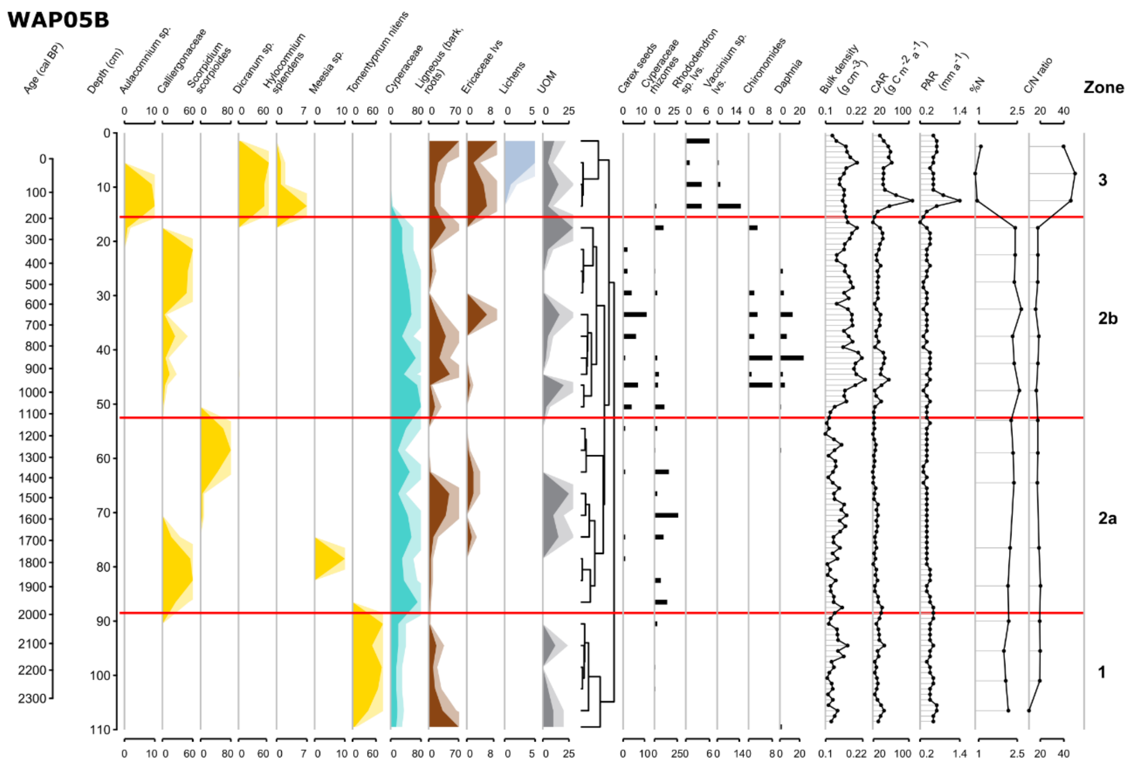

__Figure 2.__ Low Arctic polygon WAP05B. Plant macrofossil abundances (%) and counts, bulk density, carbon (CAR) and peat (PAR) accumulation rates, and peat N content (%) and C/N ratio for WAP05B. Different zones in the peat profile were identified using constrained hierarchical clustering (CONISS). Semi-transparent silhouettes represent a twofold graphical exaggeration of the plotted macrofossil abundances. UOM = Unidentified organic matter.

3.4 Paleoecological reconstructions of permafrost peatlands

3.4.1 Low Arctic tundra

At WAP05B polygonal peatland, peat thickness was 110 cm, and long-term PAR was 0.46 mm a^{-1} (**Table 1**). Peat started to accumulate around 2390 cal BP, and four main zones were identified in the plant macrofossil assemblages (**Figure 2; Table 2**). WAP05B began to develop over newly exposed mineral soil as a rich fen characterized by *Tomentypnum nitens* (zone 1; 2390–2010 cal BP), followed by two fen phases (zones 2a and 2b) characterized by Cyperaceae sedges and mosses of the family Calliergonaceae. The presence of *Scorpidium scorpioides* (zone 2a; 2010–1110 cal BP) and Chironomidae head capsules and *Daphnia* eggs (zone 2b, 1110–190 cal BP) suggests wetter conditions than during the initial *T. nitens* rich-fen phase. The most recent fen phase (zone 2b) lasted until ~190 cal BP, when bog mosses

Aulacomnium sp., *Dicranum* sp., and *Hylocomnium splendens* took over. This rapid transition to drier bog vegetation suggests permafrost aggradation during the Little Ice Age (LIA). The highest zone-specific PAR (0.67 mm a^{-1}) and CAR (51.9 g C m^{-2} a^{-1}) were recorded in zone 3 (190 cal BP to the present), which corresponds to the most recent, poorly decomposed peat (Young et al., 2019). The median N content (%) was lowest (0.94%), whereas the median C content (43.2%) and C/N ratio (45.9) were highest in zone 3.

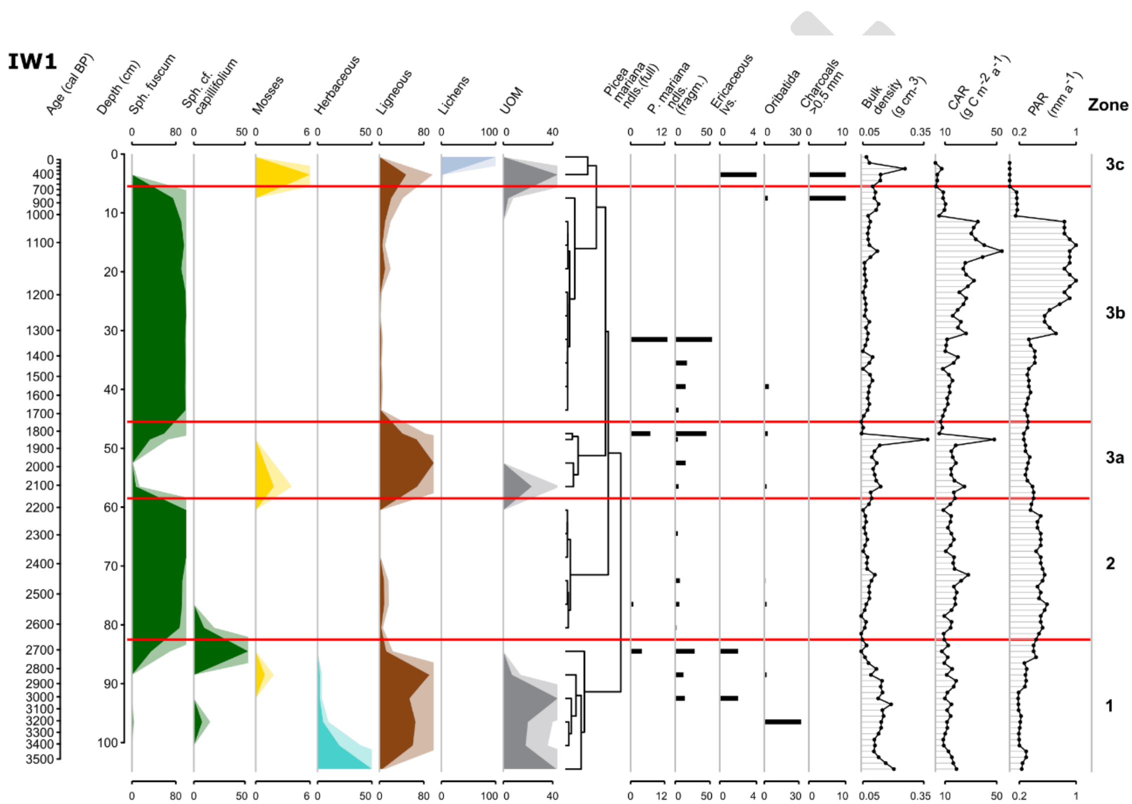

Figure 3. *Subarctic polygon IW1. Plant macrofossil abundances (%) and counts, bulk density, and carbon (CAR) and peat (PAR) accumulation rates for IW1. Different zones in the peat profile were identified using constrained hierarchical clustering (CONISS). Semi-transparent silhouettes represent a twofold graphical exaggeration of the plotted macrofossil abundances. UOM = Unidentified organic matter.*

3.4.2 Subarctic tundra

All paleoreconstruction sites in this region were polygonal peatlands, where peat started to accumulate between ~3710 and 3540 cal BP (**Table 1**).

At IW1, peat thickness was 105 cm, and peat accumulation started ~3590 cal BP, and the long-term PAR was 0.29 mm a^{-1}. Ligneous and herbaceous rootlets characterized zone 1 (3590–2670cal BP; **Figure 3**). The occurrence of *Sphagnum* cf. *capillifolium* and ericaceous leaves, as well as *Picea mariana* needles, suggests that bog development began during this initial phase. From ~2670 to 2170 cal BP (zone 2), the high abundance of *Sphagnum fuscum* and *P. mariana* needles indicates a treed bog phase. The decreased abundance of *S. fuscum* and increased abundance of ligneous material from 59 to 46 cm (zone 3a; 2170–1760 cal BP) suggests a forested phase with *P. mariana*. From ~1760 to 770 cal BP (zone 3b), the site was still dominated by *S. fuscum,* but *P. mariana* disappeared ~1330 cal BP. The presence of charcoal between 8 and 3 cm below the surface suggests a local fire between ~860 and 250 cal BP. Zone 3c (~770 cal BP to present) was characterized by mosses (mainly *Polytrichum* sp.) and *Cladonia* lichens. Peat accumulation diminished ~1050 cal BP, and the lowest zone-specific PAR (0.07 mm a^{-1}) and CAR (4.6 g C m^{-2} a^{-1}) were recorded in zone 3c, reflecting drying associated with permafrost aggradation.

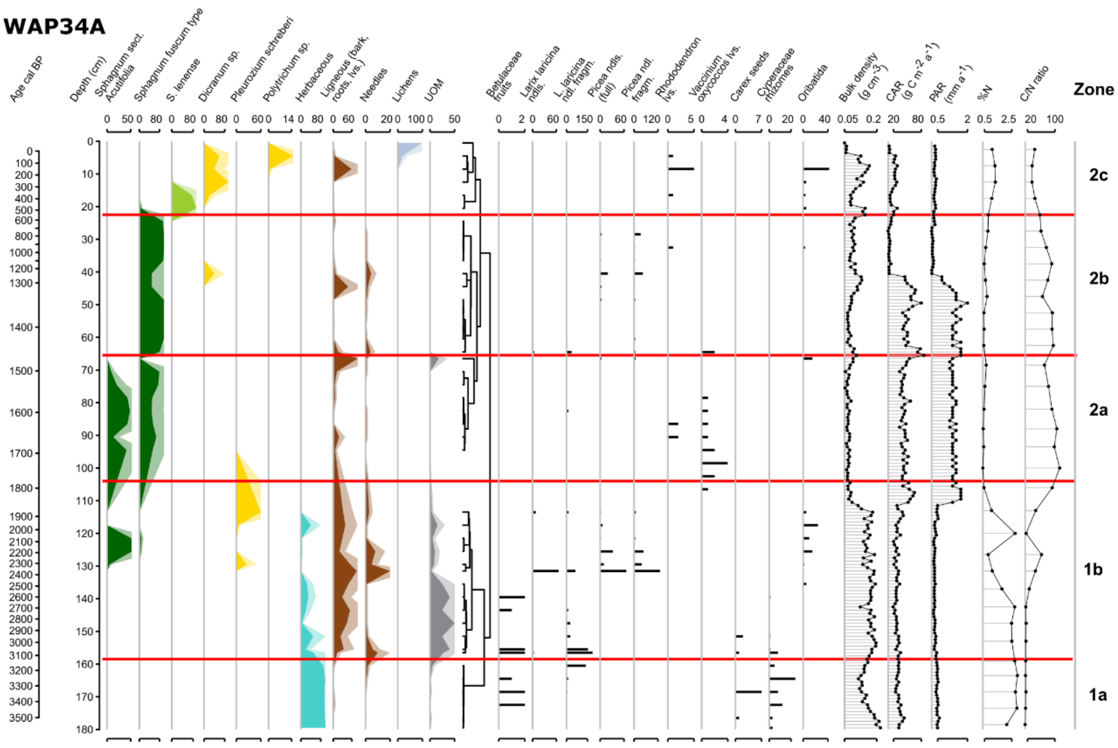

Figure 4. Subarctic polygon WAP34A. Plant macrofossil abundances (%) and counts, bulk density, carbon (CAR) and peat (PAR) accumulation rates, and peat N content (%) and C/N ratio for WAP34A. Different zones in the peat profiles were identified using constrained hierarchical clustering (CONISS).

Semi-transparent silhouettes represent a twofold graphical exaggeration of the plotted macrofossil abundances. UOM = Unidentified organic matter.

At WAP34A, peat thickness was 180 cm, and long-term PAR was 0.51 mm a^{-1} (**Table 1**). Peat accumulation began ~3540 cal BP, and five main phases were identified (**Figure 4; Table 2**). Until ~3140 cal BP (zone 1a), the site was a sedge-dominated fen or a swamp with shrubs/trees of the Betulaceae family (birch and/or alder). Between ~3140 and 1760 cal BP (zone 1b), the WAP34A site was characterized by coniferous trees and herbaceous vegetation. Initially, *Larix* co-occurred with Betulaceae species, followed by the appearance of *Picea mariana* and *P. glauca*, as well as *Pleurozium schreberi* ~2300 cal BP. The appearance of *P. mariana* also coincided with the emergence of the first *Sphagnum* mosses (section Acutifolia). From ~1760 to 1460 cal BP (zone 2a), vegetation was dominated by *S.* section *Acutifolia* (including *S. fuscum* type) and *Vaccinium oxycoccos*, indicating an open bog phase. Peat and carbon accumulation rates were the highest during this open bog phase, with zone-specific PAR of 1.31 mm a^{-1} and CAR of 43.4 g C m^{-2} a^{-}1, while median N content was the lowest (0.45%). Zone 2b (from 1460 to 570 cal BP) remained dominated by *S. fuscum* type, though the abundance of *Picea* needles suggests a treed bog phase. Peat accumulation decreased ~1270 cal BP, indicating cooling. *Picea* trees completely disappeared ~780 cal BP and *S. fuscum* type ~480 cal BP. The vegetation shifted to dominance by tundra mosses, including *S. lenense* and *Dicranum* spp., ~550 cal BP (zone 2c), suggesting permafrost aggradation. Correspondingly, the basal age of the peat core from an ice-wedge through (WAP34B) was ~570 cal BP. The lowest zone-specific PAR (0.37 mm a^{-1}) and CAR (19.6 g C m^{-2} a^{-1}) were recorded in zone 2c.

At OWL 2.1, peat thickness was 166 cm, and long-term PAR was 0.45 mm a^{-1} (**Table 1**). Peat accumulation began ~3710 cal BP. The beginning of zone 1a (3710–2710 cal BP) was characterized by sedges and *Scorpidium scorpioides*, indicating wet conditions of a moderately rich fen. Bog species *Chamaedaphne calyculata* appeared already ~3530 cal BP and *Picea* spp. (mainly *P. mariana*) ~2910 cal BP. Between 2710 and 2200 cal BP (zone 1b), OWL 2.1 was characterized by *Sphagnum* sect. *Acutifolia*, *Vaccinium oxycoccos*, and *P. mariana*, representing a treed bog phase. The highest zone-specific PAR (1.04 mm a^{-1}) and CAR (30.6 g C m^{-2} a^{-1}) were recorded for zone 1b (**Table 2**). *Larix laricina* needles increased towards the end of zone 1b. From 2200 to 460 cal BP (zone 2a), the site remained dominated by *Sphagnum* mosses and *P. mariana*, but species of *Sphagnum* sect. *Cuspidata* were also abundant. The peat accumulation rate decreased ~1530 cal BP. *P. mariana* needles were not found above 30-31 cm, dating ~890 cal BP, and some charcoals were found in the same layer. The disappearance of spruce was followed by a peak in wet-habitat species *Warnstorfia fluitans* aggr. and *Sphagnum* sect. *Cuspidata* (incl. *S. riparium*, not shown in the macrofossil diagram), suggesting that the fire event may have triggered permafrost thaw, if permafrost formed during the early LIA. Ligneous rootlets and bark, as well as remnants of lichens, peaked at 22 cm depth (~270 cal BP), possibly linked with a second phase of permafrost aggradation. From 460 cal BP to the present (zone 2b), OWL 2.1 was dominated by a tundra species, *Sphagnum lenense*, until lichens took over in the 20th century.

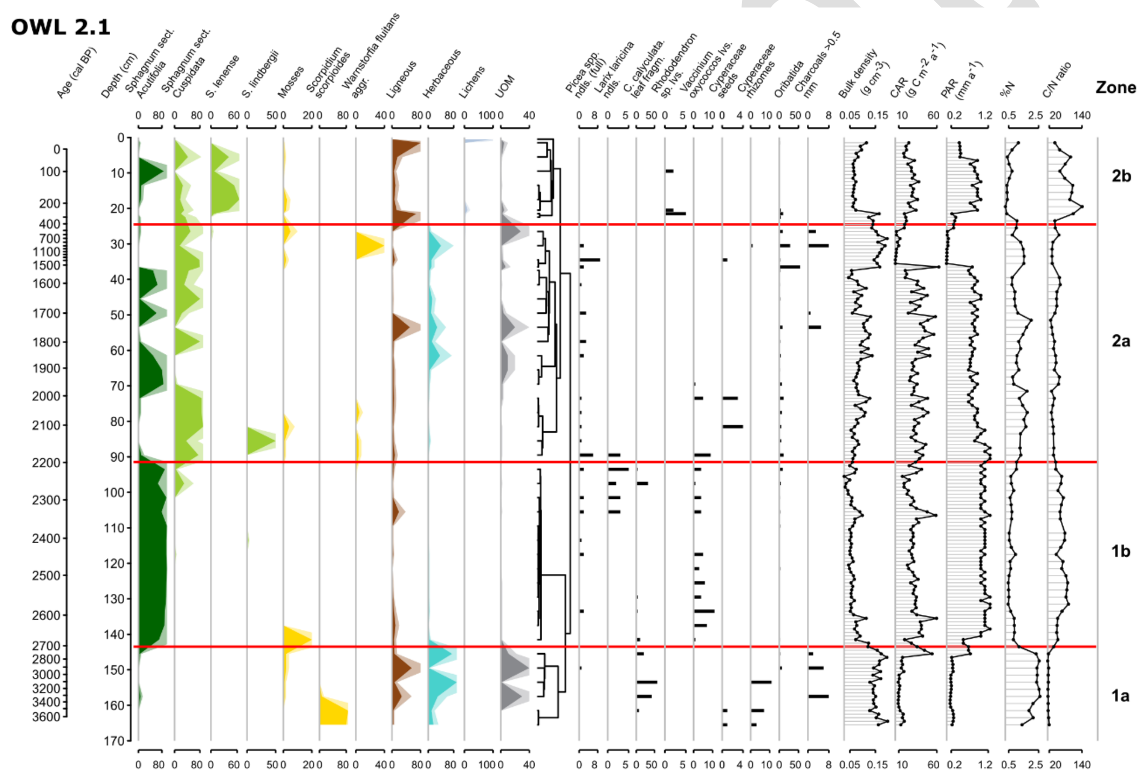

__Figure 5.__ Subarctic polygon OWL 2.1. Plant macrofossil abundances (%) and counts, bulk density, carbon (CAR) and peat (PAR) accumulation rates, and peat N content (%) and C/N ratio for OWL 2.1. Different zones in the peat profile were identified using constrained hierarchical clustering (CONISS). Semi-transparent silhouettes represent a twofold graphical exaggeration of the plotted macrofossil abundances. UOM = Unidentified organic matter.

3.4.3 Northern boreal forest

At WAP27-1B treed peat plateau, peat thickness was 251 cm, and long-term PAR was 0.44 mm a^{-1} (**Table 1**). Peatland initiation began ~5710 cal BP. However, the base of the core (286–251cm) was characterized by fluctuating layers of mineral soil and organic matter, likely reflecting glacial isostatic adjustment and sea-level fluctuations (Dalton et al. 2023; Gauthier et al., 2020). Between 5710 and 3780 cal BP (zone 1a), plant macrofossils were characterized by Betulaceae leaves and fruits, *Carex* and *Juncus* seeds, Cyperaceae rhizomes, and *Daphnia* eggs (**Figure 6**). This indicates a shrub-sedge fen phase with high water table. Calliergonaceae mosses and *Larix laricina* needles increased towards the end of this phase.

Sphagnum sect. *Acutifolia* and *Picea mariana* appeared ~3590 cal BP, characterizing zone 1b (3780–2610 cal BP). Charred *Picea* needles and charcoals were also abundant, indicating at least one wildfire ~2750 cal BP (**Table S2**). After the fire, the site was still characterized by *Sphagnum fuscum,* and *P. mariana* increased over time (zone 1c; ~2610–1600 cal BP). In contrast to the subarctic sites, zone-specific PAR was the lowest during this treed bog phase (PAR = 0.23 mm a^{-1}; **Table 2**). From ~2590 to 1760 cal BP, PAR was ca. 0.2 mm a^{-1} and CAR less than 10 g C m^{-2} a^{-1}, likely reflecting peat loss and low post-fire peat accumulation.

The next phase, from ~1600 to 780 cal BP (zone 2), was characterized by *S*. sect. *Cuspidata* and rapid peat and carbon accumulation (zone-specific PAR of 1.1 mm a^{-1} and CAR of 45.4 g C m^{-2} a^{-1} (**Table 2**). First, the landscape likely opened after a wildfire ~1500 cal BP, and *P. mariana* temporarily disappeared. Poor-fen species *Warnstorfia fluitans* and *S. jensenii* aggr. increased, suggesting high water tables. *P. mariana* increased towards 800 cal BP, when vegetation again shifted from the dominance of *S*. sect. *Cuspidata* to hummock-level species *S. fuscum* and *Vaccinium oxycoccos*. This shift marks the transition not only to drier conditions but also to slower peat accumulation (zone 3a between 780 and 30 cal BP). Around 760 cal BP, PAR dropped from 1.3 to 0.8 mm a^{-1} (**Figure 6**), suggesting permafrost aggradation. A third reconstructed fire occurred approximately 730 cal BP (**Table S2**), but *Picea* trees did not totally disappear from the site, although the number of needle fragments decreased in peat ~590 cal BP. Ericaceous shrubs (mostly *Rhododendron tomentosum*) increased ~100 cal BP. Zone 3b (~30 cal BP to the present) represents the contemporary vegetation of treed peat plateaus, dominated by *R. tomentosum* and *Cladonia* spp. lichens.

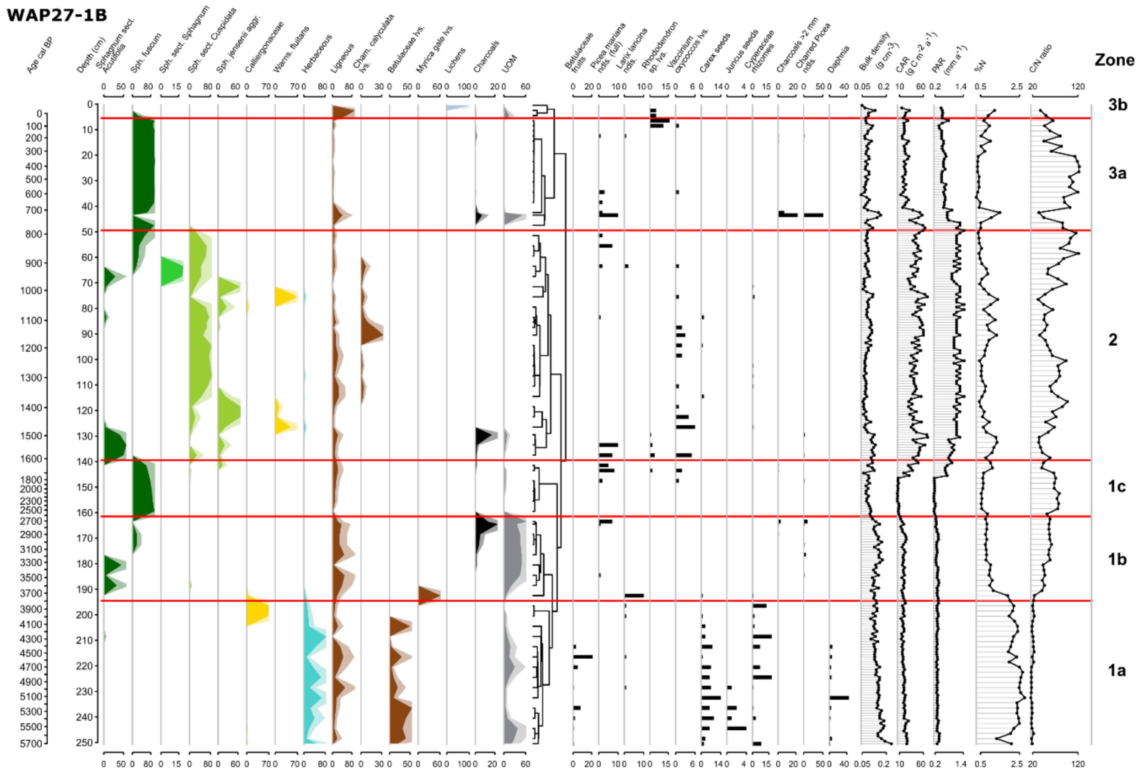

__Figure 6.__ Treed peat plateau WAP27-1B. Plant macrofossil abundances (%) and counts, bulk density, carbon (CAR) and peat (PAR) accumulation rates, and peat N content (%) and C/N ratio for WAP27-1B. Different zones in the peat profile were identified using constrained hierarchical clustering (CONISS). Semi-transparent silhouettes represent a twofold graphical exaggeration of the plotted macrofossil abundances. UOM = Unidentified organic matter.

4 Discussion

4.1 Peatland initiation and long-term carbon accumulation

Since the retreat of the Laurentide Ice Sheet and land emergence from the postglacial Tyrell Sea, peatland initiation in the HBL has been primarily governed by the influence of glacial isostatic adjustment and climate (Dredge & Mott, 2003; Glaser et al., 2004; Packalen et al., 2014). In WNP, peat thickness, age, and carbon mass increase from the coast to inland (**Table 1; Supplemental Figure S11**). Peatland initiation dates to at least 6000 cal BP in the boreal forest and extends into recent centuries along the coast, where new fens are still formed following ongoing land emergence. These same gross patterns have been found across the entire HBL complex (Dredge & Mott, 2003; Zhang et al., 2012; Packalen et al., 2014, 2016; Li et al., 2025).

Among peatland types in WNP, total C masses and long-term C accumulation rates (LORCA) were generally higher in treed/forested peat plateaus and polygonal peatlands than in non-permafrost fens, reflecting the ongoing glacial isostatic adjustment and peatland succession from coastal fens to treed peat plateaus and polygons (Korhola et al., 1995). On average, treed peat plateaus store 71.7±21.4 (SE) kg C m^{-2}, polygonal peatlands 63.2±7.14 kg C m^{-2}, and non-permafrost fens 20.4±1.75 kg C m^{-2}. These values are lower than those generally found in the HBL complex, where a mean total mass of 107 kg C m^{-2} has been reported for bogs (incl. palsas and peat plateaus) and that of 81 kg C m^{-2} for fens (Packalen et al., 2016). In addition to differences in growing season length and spatial variation in peat thickness (Packalen et al., 2016), lower C mass in WNP may be linked to permafrost aggradation and a subsequent decline in C accumulation (Camill et al., 2009; Lamarre et al., 2012; Robinson and Moore, 2000; Sannel and Kuhry, 2009). Most of these permafrost peatlands are currently covered by *Cladonia* spp. lichens that produce less biomass and decompose faster than *Sphagnum* mosses; therefore, limiting peat and C accumulation (Harris et al., 2018). Nevertheless, permafrost peatlands in WNP store a significant amount of soil carbon, some of which may be released to the atmosphere and exported to surface waters if the locally observed ice wedge degradation continues (Heffernan et al., 2024; Hugelius et al., 2020; Martin et al., 2017; Schuur et al., 2015, 2022; Treat et al., 2021; Wickham et al., 2020).

4.2 Peatland development and permafrost dynamics across different vegetation zones

We focused on comparing peatland development and permafrost dynamics between low Arctic and subarctic tundra and the northern boreal forest. Sharp declines in peat accumulation reflected cooling during the Dark Ages Cold Period (DACP; Helama et al., 2017; **Figure 7**). DACP occurred ~1550–1185 cal BP (Helama et al., 2017), with extreme cold temperatures ~1430–1230 cal BP, a period named the Late Antique Little Ice Age (LALIA; Büntgen et al., 2016; van Dijk et al., 2024). Continued low peat and C accumulation and changes in vegetation further suggest permafrost aggradation during the Little Ice Age (LIA; van Dijk et al., 2024). The LIA occurred approximately between 650 and 100 cal BP (1300–1850 CE), with evidence for a particularly cold period between 310 and 110 cal BP (1640–1840 CE; van Dijk et al., 2024). Permafrost aggradation during the LIA has also been reported from peatlands in subarctic Quebec on the eastern coast of HBL (Payette & Delwaide, 2004;

Arlen-Pouliot & Bhiry, 2005; Bhiry et al., 2007; Lamarre et al., 2012) and the sporadic permafrost zone in northern Manitoba (Camill et al., 2009). Moreover, succession trajectories differed between vegetation zones. Most importantly, the lack of fen vegetation after permafrost aggradation suggests that in the subarctic tundra, intermediate-centred polygons did not evolve from low-centred polygons, as is commonly interpreted (e.g., Mackay, 2000; Liljedahl et al., 2016; Vardy et al., 2005). Instead, our results suggest that polygonal ground formed in open peat plateaus after trees disappeared between ~1330 and 780 cal BP.

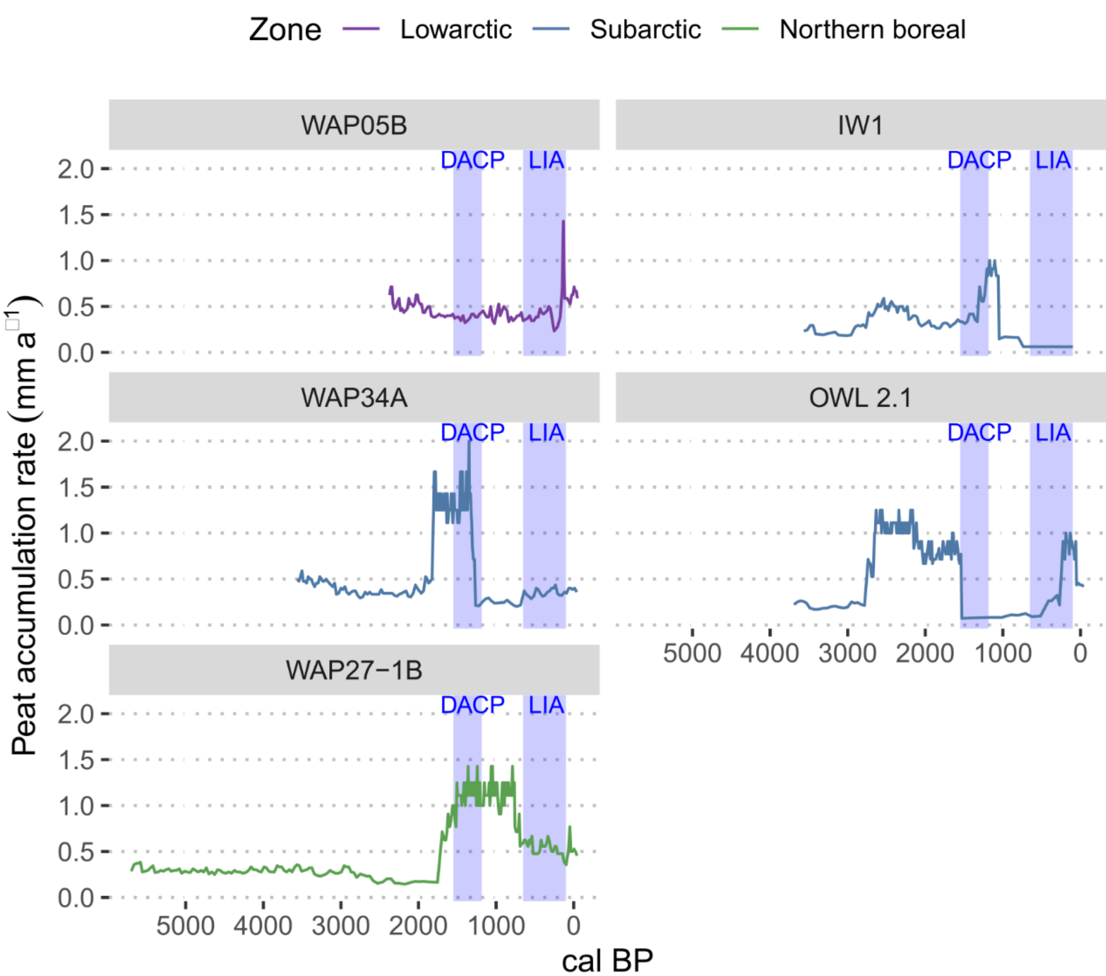

Figure 7. *Peat accumulation rate (PAR; mm a-1) since peatland initiation. At the low Arctic site WAP05B, PAR has been relatively stable over time. At the subarctic polygons (IW1, WAP34A, and OWL 2.1), PAR declined rapidly around 1530–1050 cal BP, reflecting cooling during the Dark Ages Cold Period (DACP; 1500–1185 cal BP, Helama et al., 2017) and permafrost aggradation during the Little Ice Age (LIA). At the WAP27-1B treed peat plateau in the northern boreal forest, PAR was high through DACP and decreased around 760 cal BP, suggesting permafrost aggradation at the onset of the LIA.*

4.2.1 Low Arctic tundra

At the low Arctic site WAP05B, peat began to accumulate ~2390 cal BP. Vegetation shifted from wet fen vegetation with Calliergonaceae mosses to the dominance of bog mosses (mostly *Dicranum* spp.) and dwarf shrubs ~190 cal BP, suggesting drying conditions with permafrost aggradation (Tarnocai & Zoltai, 1975; Vardy et al., 2005; Hichens-Bergström & Sannel, 2023) during the late LIA. No sharp decline in peat accumulation was observed at WAP05B, unlike in subarctic and northern boreal sites (**Figures 2 and 7; Table 3**), reflecting the effect of cooling throughout the DACP and the vegetation/peat type that preceded the present-day polygons. The peat profile from WAP05B consisted mostly of fen peat, which generally has lower peat accumulation rates than *Sphagnum* peat (Ovenden 1990; Turunen et al., 2002; Davies et al., 2021). Permafrost aggradation during the LIA is supported by a decrease in peat N content (%) and an increase in C/N ratio (Treat et al., 2016). However, the changes we observed in N% and C/N ratio at WAP05B are at least partly explained by the shift from fen to bog vegetation (Watmough et al., 2022).

In theory, intermediate-centred polygons at WAP05B could have developed from low-centred polygons. The present-day polygon was preceded by wet fen vegetation with Calliergonaceae mosses and sedges, commonly found in low-centred polygons (De Klerk et al., 2011; Mackay, 2000; Wolter et al., 2016). Multiple Chironomidae head capsules and *Daphnia* spp. resting eggs were also found in this peat layer, which dates from ~1110 to 190 cal BP (**Figure 2**), suggesting an aquatic habitat. However, dating organic material preserved within the ice wedges would be needed to constrain the timing of ice wedge formation at the low Arctic WAP05B site. At present, small and shallow ponds are common in WNP, but we have not found any low-centred polygons. Thus, we conclude that permafrost and intermediate-centred polygons formed in the low Arctic tundra during the late LIA, but the exact successional pathway remains uncertain.

4.2.2 Subarctic tundra

At subarctic polygonal peatlands in WNP (IW1, WAP34A, and OWL 2.1), peat started to accumulate on recently exposed mineral soil between 3710 and 3540 cal BP. Paleoreconstructions suggest that the shift from fen to *Sphagnum* bog vegetation occurred

~3210–2300 cal BP (**Figures 3-5; Table 3**). This shift was followed by a treed bog phase, mainly with *Sphagnum fuscum* and *Picea mariana* (and some *P. glauca*). At the WAP34A site, an open *S. fuscum* bog preceded the treed bog phase, and at OWL 2.1, vegetation shifted from the dominance of *S. fuscum type* to that of *S. sect. Cuspidata* ~2200 cal BP. It is noteworthy that peat and carbon accumulation were fast during the *Sphagnum* bog stages, suggesting non-permafrost conditions. At WAP34, for example, PAR ranged from 0.7 to 2.0 mm a^{-1} and CAR from 33.1 to 86.0 g C m^{-2} a^{-1} during 1810 –1280 cal BP (**Figures 4 and 7**). These are comparable, and in some cases exceed, the PAR and CAR values reported for boreal bogs in non-permafrost regions (e.g., Gorham et al., 2003; Jauhiainen et al., 2004; Mathijssen et al., 2016).

Peat and C accumulation rates declined rapidly between 1500 and 1050 cal BP, suggesting cooling during the DACP (Charman et al., 2013). Further on, spruce (*P. mariana* and *P. glauca*) disappeared around 890–780 cal BP at the WAP34A and OWL 2.1 sites. At IW1, spruce disappeared already ~1330 cal BP. The disappearance of spruce is likely linked to shifts toward colder climatic conditions during the DACP and later during the onset of LIA (Helama et al., 2017; Delwaide et al., 2021; van Dijk et al., 2024). Specifically, short growing seasons during the DACP and the LIA may have constrained the sexual reproduction of spruce (Meunier et al., 2007; Splawinski et al., 2022). Reduced growth of *Picea mariana* during the DACP and at the onset of the LIA has been evidenced by pollen data from marine sediments from eastern Hudson Bay (Vallerand et al., 2024) and tree-ring data from subarctic Quebec, northeastern Canada (Vallée & Payette, 2004; Arseneault et al., 2013; Gennaretti et al., 2014). Local wildfires at the end of the Medieval Warm Period (MWP; maximum temperatures ~970–770 cal BP; van Dijk et al., 2024) may have also contributed to the disappearance of trees (Camill et al., 2009). Charcoals were found in the OWL 2.1 core at a depth of 31–26 cm, while the last (most recent) *Picea* needles were observed at 31–30 cm. Based on the age-depth model, at least one wildfire occurred roughly between 900 and 500 cal BP, overlapping with the end of MWP and early LIA (van Dijk et al., 2024).

Spruce disappearance was followed by continued slow peat and C accumulation, suggesting permafrost aggradation (Camill et al., 2009; Lamarre et al., 2012; Robinson and Moore, 2000; Sannel and Kuhry, 2009) during the LIA. At WAP34A and IW1 sites, PAR ranged from 0.06 to 0.4 mm a^{-1} and CAR from 2.5 to 28.3 g C m^{-2} a^{-1} during the LIA (**Table 3**), corresponding to low accumulation rates previously reported for permafrost periods (Sannel & Kuhry, 2009; Lamarre et al., 2012; Pelletier et al., 2017). At OWL 2.1, PAR ranged from 0.1 to 1.0 mm a^{-1} and CAR from 6.9 to 36.2 g C m^{-2} a^{-1}. These wider ranges likely reflect a post-fire thaw phase, as inferred by the abundance of *Warnstorfia fluitans* (aggregate) and wet-habitat species of *Sphagnum* sect. *Cuspidata* (Arlen-Pouliot & Bhiry, 2005; Erlington et al., 2024; Kuhry, 2008; Robinson & Moore, 2000). The disappearance of spruce likely induced thinner snow covers and thereby deeper frost penetration during winter, triggering permafrost aggradation (Payette et al., 1986). Furthermore, vegetation shifted to the dominance of tundra mosses (including *Dicranum* spp., *Polytrichum* spp., and *Sphagnum lenense*) and *Cladonia* lichens ~550–420 cal BP, further supporting the interpretation of permafrost aggradation during the early LIA.

The disappearance of spruce may have also enhanced deep frost cracking and formation of ice wedge polygons in peat plateaus, as previously reported by Payette et al. (1986). The detailed evolution of ice wedges was outside the scope of our study, but the lack of fen vegetation after permafrost aggradation suggests that intermediate-centred polygons did not evolve from wet, low-centred polygons in the subarctic tundra zone. We collected and dated the base of one peat profile (WAP34B) from an ice-wedge trough. The age of the peat on top of the ice wedge was ~570 cal BP, and correspondingly, *S. lenense* replaced *S. fuscum* in the polygon centre at WAP34A between 600 and 500 cal BP. Both are hummock-forming species, and their distribution areas partly overlap, but *S. fuscum* is a more generalist bog species than *S. lenense*, which predominantly grows in arctic tundra, including dry polygon centres (Ovenden, 1982). A similar shift toward *S. lenense* dominance during the LIA was also observed at OWL 2.1. However, dating of organic material preserved within the ice wedges would be necessary to constrain the exact timing of ice-wedge formation and growth (Lachniet et al., 2012; Vasil'chuk et al., 2026). Kasper & Allard (2001) reported intense ice-wedge activity during the LIA on the eastern coast of Hudson Bay, but further research is needed on ice-wedge evolution and activity in the northwestern HBL.

4.2.3 Northern boreal forest

The development history of our treed plateau site (WAP27-1B) roughly follows the same patterns documented by Kuhry (2008) in a treed plateau approximately 20 km northwest along the Hudson Bay railroad. At WAP27-1B, peat accumulation began ~5700 cal BP, and the fen-bog transition occurred ~3590 cal BP (Figures 6 and 7; Table 3). Kuhry (2008) estimated that the first phase of permafrost aggradation may have occurred ~2250 cal BP. At WAP27-1B, PAR and CAR values were lowest during ~2590–1760 cal BP. However, a wildfire occurred in the area ~2750 cal BP, and peat loss and diminished post-fire peat accumulation may explain the low PAR and CAR values (Kuhry, 1994; Robinson & Moore, 2000; Sannel & Kuhry, 2009) rather than permafrost aggradation. In either case, northern boreal peatlands have likely remained permafrost-free from 1600 to 700 cal BP, throughout the cooling of DACP and until the onset of the LIA. This was indicated by relatively high PAR and CAR values and the abundance of wet-habitat moss species, including *Sphagnum jensenii* (aggregate) and *Warnstorfia fluitans*. PAR and CAR diminished ~760 cal BP, spruce declined ~590 cal BP, and ericaceous shrubs increased ~100 cal BP, suggesting permafrost aggradation during the LIA. Correspondingly, Kuhry (2008) concluded that in northern boreal forests of northern Manitoba, treed peat plateaus formed ~800–400 cal BP.

Conclusions

Paleoreconstructions from peatlands in the northwestern Hudson Bay Lowlands suggest relatively recent permafrost aggradation in the region. Peat and carbon accumulation rates generally declined between ~1530 and 760 cal BP, coinciding with cooling from the Dark Ages Cold Period to the Little Ice Age. Spruce (*Picea mariana, P. glauca*) disappeared from the subarctic peatlands and decreased at the northern boreal peatland between 1330 and 590 cal BP. Taken together, the abrupt decline in peat and carbon accumulation rates following periods of rapid accumulation, spruce disappearance, and the shift to vegetation of open peat plateaus and polygonal peatlands suggests permafrost aggradation across the northwestern Hudson Bay Lowlands during the Little Ice Age. Subsequently, permafrost remained relatively stable, except for a short thaw phase following a wildfire at the subarctic OWL 2.1 site. However, due to its relatively recent origin, permafrost in the region may be particularly vulnerable to thaw under present warming.

Our paleoecological reconstructions further suggest that in the subarctic tundra, dry intermediate-centred polygons did not evolve from wet, low-centred polygons, as commonly interpreted. Instead, ice wedge polygons appear to have developed in *Sphagnum*-dominated peat plateaus, following the disappearance of spruce. In the low Arctic tundra, however, the study site was characterized by fen vegetation until the Little Ice Age, when dry intermediate-centred polygons developed, but the exact successional pathway remains uncertain. These contrasting histories highlight the importance of considering peatland development and the type of permafrost peat when assessing the vulnerability of permafrost and potential climate-carbon feedbacks in a warming climate.

CRediT author statement

All authors contributed substantially to data collection and reviewed and approved the final version of the manuscript. The authors also contributed to the following tasks: Conceptualization (THMK, MG, LG, FB), Methodology (THMK, MG, NKS, LG), Writing – original draft (THMK), Writing – review and editing (MG, LG, JA, MB, FB, LAF, NKS, AEC, AC, LCW, SF), Visualization (THMK, AC), Supervision (MG, NKS), Project administration (MG, AEC, KR), Funding acquisition (MG, KR, LG, FB).

Declaration of competing interest

The authors declare that they have no competing interests.

Acknowledgments

This work was supported by funding from Parks Canada and ANR grant (Arctic-Peat, no. ANR 2020 – CE01-001) to LG. The work of FB, JA, and LCW was supported by NSERC Discovery and Northern Research Supplement funding, Polar Continental Shelf Program (PCSP), and Northern Research Fund (NRF) from Churchill Northern Studies Centre (CNSC). We thank the Parks Canada field unit staff in Churchill for support during field campaigns, especially Erica Gillis, Nicole Rogowsky, Jesse Shirton, and Russell Turner. We thank Seal River Guardians Calvin Clipping, Sadie Dumas, and Augustine Tessessage for their assistance in collecting peat cores. We are grateful to Joëlle Cormier, Gauthier Genez, Raphaëlle Grégoire, and

Guillaume Provost for their assistance in laboratory work. We also appreciate the support of Léonie Perrier during this project. We acknowledge the PAPC platform at the CRBE laboratory (France) and the light stable isotope geochemistry laboratory at Geotop-UQAM (Canada) for C and N analysis. Fieldwork in the Churchill Wildlife Management Area was conducted under permits 78303365 (2024) and 90026228 (2025) from Manitoba Conservation.

References

Abolt, C. J., Young, M. H., Atchley, A. L., Harp, D. R., & Coon, E. T. (2020). Feedbacks between surface deformation and permafrost degradation in ice wedge polygons, Arctic Coastal Plain, Alaska. *Journal of Geophysical Research: Earth Surface, 125*(3), e2019JF005349. https://doi.org/10.1029/2019JF005349

Arlen-Pouliot, Y., & Bhiry, N. (2005). Palaeoecology of a palsa and a filled thermokarst pond in a permafrost peatland, subarctic Québec, Canada. *The Holocene, 15*(3), 408-419. https://doi.org/10.1191/0959683605hl818r

Ayoutte, G. & Rochefort, L. (2019). Les sphaignes de l'Est du Canada – Clé d'identification visuelle et cartes de répartition. Les Éditions JFD Inc., Montréal, Québec, Canada. ISBN: 978-2-924651-99-5

Baldwin, K., Allen, L., Basquill, S., Chapman, K., Downing, D., Flynn, N., MacKenzie, W., Major, M., Meades, W., Meidinger, D., Morneau, C., Saucier, J-P., Thorpe, J., Uhlig, P. (2019). Vegetation Zones of Canada: a Biogeoclimatic Perspective. [Map] Scale 1:5,000,000. *Natural Resources Canada, Canadian Forest Service. Great Lake Forestry Center, Sault Ste. Marie, ON, Canada*.

Bhiry, N., Payette, S., & Robert, É. C. (2007). Peatland development at the arctic tree line (Québec, Canada) influenced by flooding and permafrost. *Quaternary Research*, *67*(3), 426-437. https://doi.org/10.1016/j.yqres.2006.11.009

Biskaborn, B. K., Smith, S. L., Noetzli, J, Matthes, H., Vieira, G., Streletskiy, D. A., ... & Lantuit, H. (2019). Permafrost is warming at a global scale. *Nature communications*, *10*(1), 264. https://doi.org/10.1038/s41467-018-08240-4

Blaauw, M. & Christen, J.A. (2011). Flexible paleoclimate age-depth models using an autoregressive gamma process. *Bayesian Analysis, 6*(3), 457-474. https://doi.org/10.1214/11-BA618

Bouchard, F., Turner, K. W., MacDonald, L. A., Deakin, C., White, H., Farquharson, N., ... & Edwards, T. W. D. (2013). Vulnerability of shallow subarctic lakes to evaporate and desiccate when snowmelt runoff is low. *Geophysical Research Letters, 40*(23), 6112-6117. https://doi.org/10.1002/2013GL058635

Bronk Ramsey, C. (2009). Bayesian analysis of radiocarbon dates. *Radiocarbon, 51*(1), 337-360. https://doi.org/10.1017/S0033822200033865

Büntgen, U., Myglan, V. S., Ljungqvist, F. C., McCormick, M., Di Cosmo, N., Sigl, M., Jungclaus. J., Wagner, S., Krusic, P. J., Esper, J., Kaplan, J. O., de Vaan, M. A., C., Luterbacher, J., Wacker, L., Tegel, W., & Kirdyanov, A. V. (2016). Cooling and societal change during the Late Antique Little Ice Age from 536 to around 660 AD. *Nature Geoscience*, *9*(3), 231-236. https://doi.org/10.1038/ngeo2652

Camill, P., Barry, A., Williams, E., Andreassi, C., Limmer, J., & Solick, D. (2009). Climate-vegetation-fire interactions and their impact on long-term carbon dynamics in a boreal peatland landscape in northern Manitoba, Canada. *Journal of Geophysical Research: Biogeosciences, 114*(G4). https://doi.org/10.1029/2009JG001071

Cassidy A. E., Kolari, T. H. M., Collingwood, A., Richardson, K., ..., & Garneau, M. Mapping carbon stocks across peatlands in Wapusk National Park. (*manuscript in prep.*)

Chambers, F. M., Beilman, D. W., & Yu, Z. (2011). Methods for determining peat humification and for quantifying peat bulk density, organic matter and carbon content for palaeostudies of climate and peatland carbon dynamics. *Mires and peat, 7,* 07.

Charman, D. J., Beilman, D. W., Blaauw, M., Booth, R. K., Brewer, S., Chambers, F. M., ... & Zhao, Y. (2013). Climate-related changes in peatland carbon accumulation during the last millennium. *Biogeosciences*, *10*(2), 929-944. https://doi.org/10.5194/bg-10-929-2013

Dalton, A. S., Dulfer, H. E., Margold, M., Heyman, J., Clague, J. J., Froese, D. G., Gauthier, M. S., Hughes, A. L. C., Jennings, C. E., Norris, S. L., & Stoker, B. J. (2023). Deglaciation of the north American ice sheet complex in calendar years based on a comprehensive database of chronological data: NADI-1. *Quaternary Science Reviews, 321*, 108345. https://doi.org/10.1016/j.quascirev.2023.108345

De Klerk, P., Donner, N., Karpov, N. S., Minke, M., & Joosten, H. (2011). Short-term dynamics of a low-centred ice-wedge polygon near Chokurdakh (NE Yakutia, NE Siberia) and climate change during the last ca 1250 years. *Quaternary Science Reviews, 30*(21-22), 3013-3031. https://doi.org/10.1016/j.quascirev.2011.06.016

Dearborn, K. D., Wallace, C. A., Patankar, R., & Baltzer, J. L. (2021). Permafrost thaw in boreal peatlands is rapidly altering forest community composition. *Journal of Ecology*, *109*(3), 1452-1467. https://doi.org/10.1111/1365-2745.13569

Delwaide, A., Asselin, H., Arseneault, D., Lavoie, C., & Payette, S. (2021). A 2233-year tree-ring chronology of subarctic black spruce (Picea mariana): growth forms response to long-term climate change. *Ecoscience, 28*(3-4), 399-419. https://doi.org/10.1080/11956860.2021.1952014

Dredge, L. A., & Mott, R. J. (2003). Holocene pollen records and peatland development, northeastern Manitoba. *Géographie physique et Quaternaire, 57*(1), 7-19. https://doi.org/10.7202/010328ar

Ellis, C. J., Rochefort, L., Gauthier, G., & Pienitz, R. (2008). Paleoecological evidence for transitions between contrasting landforms in a polygon-patterned High Arctic wetland.

Arctic, Antarctic, and Alpine Research, 40(4), 624-637. https://doi.org/10.1657/1523-0430(07-059)[ELLIS]2.0.CO;2

Errington, R. C., Macdonald, S. E., & Bhatti, J. S. (2024). Rate of permafrost thaw and associated plant community dynamics in peatlands of northwestern Canada. *Journal of Ecology, 112*(7), 1565-1582. https://doi.org/10.1111/1365-2745.14339

Faubert, J. (2014). Flore des bryophytes du Québec-Labrador. Volume 3 : Mousses, seconde partie. Société québécoise bryologie, Saint-Valérien, Québec, Canada. 456 p. ISBN : 978-2-9813260-2-7

Fortier, D., & Allard, M. (2005). Frost-cracking conditions, Bylot Island, eastern Canadian Arctic archipelago. *Permafrost and Periglacial Processes, 16*(2), 145-161. https://doi.org/10.1002/ppp.504

Fritz, M., Wolter, J., Rudaya, N., Palagushkina, O., Nazarova, L., Obu, J., ... & Wetterich, S. (2016). Holocene ice-wedge polygon development in northern Yukon permafrost peatlands (Canada). *Quaternary Science Reviews, 147*, 279-297. https://doi.org/10.1016/j.quascirev.2016.02.008

Gauthier, M. S., Kelley, S. E., & Hodder, T. J. (2020). Lake Agassiz drainage bracketed Holocene Hudson Bay ice saddle collapse. *Earth and Planetary Science Letters, 544,* 116372. https://doi.org/10.1016/j.epsl.2020.116372

Gennaretti, F., Arseneault, D., Nicault, A., Perreault, L., & Bégin, Y. (2014). Volcano-induced regime shifts in millennial tree-ring chronologies from northeastern North America. *Proceedings of the National Academy of Sciences*, *111*(28), 10077-10082. https://doi.org/10.1073/pnas.1324220111

Glaser, P. H., Hansen, B. C., Siegel, D. I., Reeve, A. S., & Morin, P. J. (2004). Rates, pathways and drivers for peatland development in the Hudson Bay Lowlands, northern Ontario, Canada. *Journal of Ecology, 92*(6), 1036-1053. https://doi.org/10.1111/j.0022-0477.2004.00931.x

Gorham, E., Janssens, J. A., & Glaser, P. H. (2003). Rates of peat accumulation during the postglacial period in 32 sites from Alaska to Newfoundland, with special emphasis on northern Minnesota. *Canadian Journal of Botany*, *81*(5), 429-438. https://doi.org/10.1139/b03-036

Harris, L. I., Moore, T. R., Roulet, N. T., & Pinsonneault, A. J. (2018). Lichens: A limit to peat growth? *Journal of Ecology, 106*(6), 2301-2319. https://doi.org/10.1111/1365-2745.12975

Heffernan, L., Kothawala, D. N., & Tranvik, L. J. (2024). Terrestrial dissolved organic carbon in northern permafrost. *The Cryosphere, 18*(3), 1443-1465. https://doi.org/10.5194/tc-18-1443-2024

Helama, S., Jones, P. D., & Briffa, K. R. (2017). Dark Ages Cold Period: A literature review and directions for future research. *The Holocene, 27*(10), 1600-1606. https://doi.org/10.1177/0959683617693898

Hichens-Bergström, M., & Sannel, A. B. K. (2023). Permafrost development in northern Fennoscandian peatlands since the mid-Holocene. *Arctic, Antarctic, and Alpine Research*, *55*(1), 2250035. https://doi.org/10.1080/15230430.2023.2250035

Hugelius, G., Loisel, J., Chadburn, S., Jackson, R. B., Jones, M., MacDonald, G., Marushchak, M., Olefeldt, D., Packalen, M., Siewert, M. B., Treat, C., Turetsky, M., Voigt, C., & Yu, Z. (2020). Large stocks of peatland carbon and nitrogen are vulnerable to permafrost thaw. *Proceedings of the National Academy of Sciences, 117*(34), 20438-20446. https://doi.org/10.1073/pnas.1916387117

Jauhiainen, S., Pitkänen, A., & Vasander, H. (2004). Chemostratigraphy and vegetation in two boreal mires during the Holocene. *The Holocene*, *14*(5), 769-779. https://doi.org/10.1191/0959683604hl734rp

Jones, M. C., Grosse, G., Treat, C., Turetsky, M., Anthony, K. W., & Brosius, L. (2023). Past permafrost dynamics can inform future permafrost carbon-climate feedbacks. *Communications Earth & Environment, 4*(1), 272. https://doi.org/10.1038/s43247-023-00886-3

Jorgenson, M. T., Kanevskiy, M. Z., Jorgenson, J. C., Liljedahl, A., Shur, Y., Epstein, H., Kent, K., Griffin, C. G., Daanen, R., Boldenow, M., Orndal, K., Witharana, C., & Jones, B. M. (2022). Rapid transformation of tundra ecosystems from ice-wedge degradation. *Global and Planetary Change, 216*, 103921. https://doi.org/10.1016/j.gloplacha.2022.103921

Jorgenson, M. T., Shur, Y. L., & Pullman, E. R. (2006). Abrupt increase in permafrost degradation in Arctic Alaska. *Geophysical Research Letters, 33*(2). https://doi.org/10.1029/2005GL024960

Juggins, S. (2024) rioja: Analysis of Quaternary Science Data, R package version (1.0-7). https://cran.r-project.org/package=rioja

Juggins, S. (2025) riojaPlot: Stratigraphic diagrams in R, package version (0.1-24). https://github.com/nsj3/riojaPlot

Kanevskiy, M., Shur, Y., Jorgenson, T., Brown, D. R., Moskalenko, N., Brown, J., Walker, D. A., Raynolds, M. K., & Buchhorn, M. (2017). Degradation and stabilization of ice wedges: Implications for assessing risk of thermokarst in northern Alaska. *Geomorphology, 297*, 20-42. https://doi.org/10.1016/j.geomorph.2017.09.001

Kasper, J. N., & Allard, M. (2001). Late-Holocene climatic changes as detected by the growth and decay of ice wedges on the southern shore of Hudson Strait, northern Québec, Canada. *The Holocene, 11*(5), 563-577. https://doi.org/10.1191/095968301680223512

Kirkwood, J. A. H., Roy-Léveillée, P., Mykytczuk, N., Packalen, M., McLaughlin, J., Laframboise, A., & Basiliko, N. (2021). Soil microbial community response to permafrost degradation in palsa fields of the Hudson Bay Lowlands: Implications for greenhouse gas production in a warming climate. *Global Biogeochemical Cycles, 35*(6), e2021GB006954. https://doi.org/10.1029/2021GB006954

Korhola, A., Tolonen, K., Turunen, J., & Jungner, H. (1995). Estimating long-term carbon accumulation rates in boreal peatlands by radiocarbon dating. *Radiocarbon, 37*(2), 575-584. https://doi.org/10.1017/S0033822200031064

Kuhry, P. (1994). The role of fire in the development of *Sphagnum*-dominated peatlands in western boreal Canada. *Journal of Ecology*, 899-910.

Kuhry, P. (2008). Palsa and peat plateau development in the Hudson Bay Lowlands, Canada: timing, pathways and causes. *Boreas, 37*(2), 316-327. https://doi.org/10.1111/j.1502-3885.2007.00022.x

Lachniet, M. S., Lawson, D. E., & Sloat, A. R. (2012). Revised 14C dating of ice wedge growth in interior Alaska (USA) to MIS 2 reveals cold paleoclimate and carbon recycling in ancient permafrost terrain. *Quaternary Research, 78*(2), 217-225. https://doi.org/10.1016/j.yqres.2012.05.007

Laine, J., Harju, P., Timonen, T., Laine, A., Tuittila, E.-S., Minkkinen, K., & Vasander, H. (2009). The Intricate Beauty of Sphagnum Mosses – A Finnish Guide to Identification. University of Helsinki Department of Forest Ecology Publications, *39,* 1-190. ISBN: 978-952-10-5617-8

Lamarre, A., Garneau, M., & Asnong, H. (2012). Holocene paleohydrological reconstruction and carbon accumulation of a permafrost peatland using testate amoeba and macrofossil analyses, Kuujjuarapik, subarctic Québec, Canada. *Review of Palaeobotany and Palynology, 186,* 131-141. https://doi.org/10.1016/j.revpalbo.2012.04.009

Langer, M., Nitzbon, J., Groenke, B., Assmann, L. M., Schneider von Deimling, T., Stuenzi, S. M., & Westermann, S. (2024). The evolution of Arctic permafrost over the last 3 centuries from ensemble simulations with the CryoGridLite permafrost model. *The Cryosphere, 18*(1), 363-385. https://doi.org/10.5194/tc-18-363-2024

Li, Y., Han, D., Rogers, C. A., Finkelstein, S. A., Hararuk, O., Waddington, J. M., Barreto, C., McLaughlin, J. W., Snider, J., & Gonsamo, A. (2025). Peat depth and carbon storage of the Hudson Bay Lowlands, Canada. *Geophysical Research Letters, 52*(2), e2024GL110679. https://doi.org/10.1029/2024GL110679

Liljedahl, A. K., Boike, J., Daanen, R. P., Fedorov, A. N., Frost, G. V., Grosse, G., Hinzman, L. D., Iijma, Y., Jorgenson, J. C., Matveyeva, N., Necsoiu, M., Raynolds, M. K., Romanovsky, V. E., Schulla, J., Tape, K. D., Walker, D. A., Wilson, C. J., Yabuki, H., & Zona, D. (2016). Pan-Arctic ice-wedge degradation in warming permafrost and its influence on tundra hydrology. *Nature Geoscience, 9*(4), 312-318. https://doi.org/10.1038/ngeo2674

Loisel, J., Yu, Z., Beilman, D. W., Camill, P., Alm, J., Amesbury, M. J., ... & Zhou, W. (2014). A database and synthesis of northern peatland soil properties and Holocene carbon and nitrogen accumulation. *The Holocene, 24*(9), 1028-1042. https://doi.org/10.1177/0959683614538073

Mackay, J. R. (1993). Air temperature, snow cover, creep of frozen ground, and the time of ice-wedge cracking, western Arctic coast. *Canadian Journal of Earth Sciences, 30*(8), 1720-1729. https://doi.org/10.1139/e93-151

Mackay, J. R. (2000). Thermally induced movements in ice-wedge polygons, western Arctic coast: a long-term study. *Géographie physique et Quaternaire, 54*(1), 41-68. https://doi.org/10.7202/004846ar

Martin, A. F., Lantz, T. C., & Humphreys, E. R. (2017). Ice wedge degradation and CO_2 and CH_4 emissions in the Tuktoyaktuk Coastlands, Northwest Territories. *Arctic Science, 4*(1), 130-145. https://doi.org/10.1139/as-2016-0011

Mauquoy, D., Hughes, P. D. M., & Van Geel, B. (2010). A protocol for plant macrofossil analysis of peat deposits. *Mires and Peat, 7,* 06.

Meunier, C., Sirois, L., & Bégin, Y. (2007). Climate and *Picea mariana* seed maturation relationships: a multi-scale perspective. *Ecological Monographs, 77*(3), 361-376. https://doi.org/10.1890/06-1543.1

Millard, A. R. (2014). Conventions for reporting radiocarbon determinations. *Radiocarbon, 56*(2), 555-559. https://doi.org/10.2458/56.17455

Obu, J., Westermann, S., Bartsch, A., Berdnikov, N., Christiansen, H. H., Dashtseren, A., ... & Zou, D. (2019). Northern Hemisphere permafrost map based on TTOP modelling for 2000–2016 at 1 km^2 scale. *Earth-Science Reviews, 193*, 299-316. https://doi.org/10.1016/j.earscirev.2019.04.023

Ouzilleau Samson, D., Bhiry, N., & Lavoie, M. (2010). Late-Holocene palaeoecology of a polygonal peatland on the south shore of Hudson Strait, northern Québec, Canada. *The Holocene, 20*(4), 525-536. https://doi.org/10.1177/095968360935658

Ovenden, L. (1982). Vegetation history of a polygonal peatland, northern Yukon. *Boreas, 11*(3), 209-224. https://doi.org/10.1111/j.1502-3885.1982.tb00715.x

Ovenden, L. (1990). Peat accumulation in northern wetlands. *Quaternary Research*, *33*(3), 377-386. https://doi.org/10.1016/0033-5894(90)90063-Q

Packalen, M. S., Finkelstein, S. A., & McLaughlin, J. W. (2014). Carbon storage and potential methane production in the Hudson Bay Lowlands since mid-Holocene peat initiation. *Nature communications, 5*(1), 4078. https://doi.org/10.1038/ncomms5078

Packalen, M. S., Finkelstein, S. A., & McLaughlin, J. W. (2016). Climate and peat type in relation to spatial variation of the peatland carbon mass in the Hudson Bay Lowlands, Canada. *Journal of Geophysical Research: Biogeosciences, 121*(4), 1104-1117. https://doi.org/10.1002/2015JG002938

Parmentier, F. J. W., Nilsen, L., Tømmervik, H., Meisel, O. H., Bröder, L., Vonk, J. E., Westermann, S., Semenchuk, P. R., & Cooper, E. J. (2024). Rapid ice-wedge collapse and permafrost carbon loss triggered by increased snow depth and surface runoff. *Geophysical Research Letters, 51*(11), e2023GL108020. https://doi.org/10.1029/2023GL108020

Payette, S., & Delwaide, A. (2004). Dynamics of subarctic wetland forests over the past 1500 years. *Ecological Monographs, 74*(3), 373-391. https://doi.org/10.1890/03-4033

Payette, S., Gauthier, L. & Grenier, I. (1986). Dating ice-wedge growth in subarctic peatlands following deforestation. *Nature, 322*, 724–727. https://doi.org/10.1038/322724a0

Pelletier, N., Talbot, J., Olefeldt, D., Turetsky, M., Blodau, C., Sonnentag, O., & Quinton, W. L. (2017). Influence of Holocene permafrost aggradation and thaw on the paleoecology and carbon storage of a peatland complex in northwestern Canada. *The Holocene, 27*(9), 1391-1405. https://doi.org/10.1177/0959683617693899

Ponomarenko, S., Quirouette, J., Sharma, R. and D. McLennan. (2014). Ecotype Mapping Report for Wapusk National Park. Monitoring and Ecological Information. *Natural Resource Conservation. Parks Canada. Gatineau, QC, Canada.*

Rantanen, M., Karpechko, A. Y., Lipponen, A., Nordling, K., Hyvärinen, O., Ruosteenoja, K., Vihma, T., & Laaksonen, A. (2022). The Arctic has warmed nearly four times faster than the globe since 1979. *Communications earth & environment, 3*(1), 168. https://doi.org/10.1038/s43247-022-00498-3

R Core Team (2025). R: A Language and Environment for Statistical Computing. R Foundation for Statistical Computing, Vienna, Austria. https://www.R-project.org

Reimer, P. J., Austin, W. E., Bard, E., Bayliss, A., Blackwell, P. G., Bronk Ramsey, C., ... & Talamo, S. (2020). The IntCal20 Northern Hemisphere radiocarbon age calibration curve (0–55 cal kBP). *Radiocarbon, 62*(4), 725-757. https://doi.org/10.1017/RDC.2020.41

Robinson, S. D., & Moore, T. R. (2000). The influence of permafrost and fire upon carbon accumulation in high boreal peatlands, Northwest Territories, Canada. *Arctic, Antarctic, and Alpine Research, 32*(2), 155-166. https://doi.org/10.1080/15230430.2000.12003351

Sannel, A. B. K., & Kuhry, P. (2008). Long-term stability of permafrost in subarctic peat plateaus, west-central Canada. *The Holocene, 18*(4), 589-601. https://doi.org/10.1177/0959683608089658

Sannel, A. B. K., & Kuhry, P. (2009). Holocene peat growth and decay dynamics in sub-arctic peat plateaus, west-central Canada. *Boreas, 38*(1), 13-24. https://doi.org/10.1111/j.1502-3885.2008.00048.x

Sella, G. F., Stein, S., Dixon, T. H., Craymer, M., James, T. S., Mazzotti, S., & Dokka, R. K. (2007). Observation of glacial isostatic adjustment in “stable” North America with GPS. *Geophysical Research Letters, 34*(2). https://doi.org/10.1029/2006GL027081

Schirrmeister, L., Bobrov, A., Raschke, E., Herzschuh, U., Strauss, J., Pestryakova, L. A., & Wetterich, S. (2018). Late Holocene ice-wedge polygon dynamics in northeastern Siberian coastal lowlands. *Arctic, Antarctic, and Alpine Research, 50*(1), e1462595. https://doi.org/10.1080/15230430.2018.1462595

Schulze, C., Sonnentag, O., Emmerton, C. A., Harris, L., Alcock, H., Marouelli, K., Hould Gosselin, G., Knox, S. H., Howard, R., Skeeter, J., Moore, P., Nesic, Z., & Olefeldt, D. (2025). Large carbon losses from burned permafrost peatlands during post-fire succession.

Geophysical Research Letters, 52(19), e2025GL118344. https://doi.org/10.1029/2025GL118344

Schuur, E. A., Abbott, B. W., Commane, R., Ernakovich, J., Euskirchen, E., Hugelius, G., ... & Turetsky, M. (2022). Permafrost and climate change: carbon cycle feedbacks from the warming Arctic. *Annual Review of Environment and Resources, 47*(1), 343-371. https://doi.org/10.1146/annurev-environ-012220-011847

Schuur, E. A., McGuire, A. D., Schädel, C., Grosse, G., Harden, J. W., Hayes, D. J., ... & Vonk, J. E. (2015). Climate change and the permafrost carbon feedback. *Nature, 520*(7546), 171-179. https://doi.org/10.1038/nature14338

Shur, Y., Jones, B. M., Jorgenson, M. T., Kanevskiy, M. Z., Liljedahl, A., Walker, D. A., Ward Jones, M. K., Fortier, D., & Vasiliev, A. (2025). Formation of Low-Centered Ice-Wedge Polygons and Their Orthogonal Systems: A Review. *Geosciences, 15*(7), 249. https://doi.org/10.3390/geosciences15070249

Shur, Y. L., & Jorgenson, M. T. (2007). Patterns of permafrost formation and degradation in relation to climate and ecosystems. *Permafrost and Periglacial Processes, 18*(1), 7-19. https://doi.org/10.1002/ppp.582

Smith, S. L., O'Neill, H. B., Isaksen, K., Noetzli, J., & Romanovsky, V. E. (2022). The changing thermal state of permafrost. *Nature Reviews Earth & Environment, 3*(1), 10-23. https://doi.org/10.1038/s43017-021-00240-1

Splawinski, T. B., Boucher, Y., Bouchard, M., Greene, D. F., Gauthier, S., Auger, I., ... & Bergeron, Y. (2022). Factors influencing black spruce reproductive potential in the northern boreal forest of Quebec. *Canadian Journal of Forest Research*, *52*(12), 1499-1512. https://doi.org/10.1139/cjfr-2022-0092

Teltewskoi, A., Beermann, F., Beil, I., Bobrov, A., De Klerk, P., Lorenz, S., Lorenz, S., Lüder, A., Michaelis, D., & Joosten, H. (2016). 4000 years of changing wetness in a permafrost polygon peatland (Kytalyk, NE Siberia): A comparative high-resolution multi-proxy study. *Permafrost and Periglacial Processes, 27*(1), 76-95. https://doi.org/10.1002/ppp.1869

Treat, C. C., Jones, M. C., Camill, P., Gallego-Sala, A., Garneau, M., Harden, J. W., ... & Väliranta, M. (2016). Effects of permafrost aggradation on peat properties as determined from a pan-Arctic synthesis of plant macrofossils. *Journal of Geophysical Research: Biogeosciences, 121*(1), 78-94. https://doi.org/10.1002/2015JG003061

Treat, C. C., & Jones, M. C. (2018). Near-surface permafrost aggradation in Northern Hemisphere peatlands shows regional and global trends during the past 6000 years. *The Holocene, 28*(6), 998-1010. https://doi.org/10.1177/0959683617752858

Treat, C. C., Jones, M. C., Alder, J., Sannel, A. B. K., Camill, P., & Frolking, S. (2021). Predicted vulnerability of carbon in permafrost peatlands with future climate change and permafrost thaw in Western Canada. *Journal of Geophysical Research: Biogeosciences*, *126*(5), e2020JG005872. https://doi.org/10.1029/2020JG005872

Turetsky, M. R., Bond-Lamberty, B., Euskirchen, E., Talbot, J., Frolking, S., McGuire, A. D., & Tuittila, E. S. (2012). The resilience and functional role of moss in boreal and arctic ecosystems. *New Phytologist*, *196*(1), 49-67. https://doi.org/10.1111/j.1469-8137.2012.04254.x

Turunen, J., Tomppo, E., Tolonen, K., & Reinikainen, A. (2002). Estimating carbon accumulation rates of undrained mires in Finland–application to boreal and subarctic regions. *The Holocene, 12*(1), 69-80. https://doi.org/10.1191/0959683602hl522rp

van Dijk, E. J., Jungclaus, J., Sigl, M., Timmreck, C., & Krüger, K. (2024). High-frequency climate forcing causes prolonged cold periods in the Holocene. *Communications Earth & Environment, 5*(1), 242. https://doi.org/10.1038/s43247-024-01380-0

Vallerand, J., de Vernal, A., & Roy, N. (2024). Climate variations in eastern Hudson Bay over the past 3000 years. *Quaternary Science Reviews, 339,* 108862. https://doi.org/10.1016/j.quascirev.2024.108862

Vallée, S., & Payette, S. (2004). Contrasted growth of black spruce (Picea mariana) forest trees at treeline associated with climate change over the last 400 years. *Arctic, Antarctic, and Alpine Research, 36*(4), 400-406. https://doi.org/10.1657/1523-0430(2004)036[0400:CGOBSP]2.0.CO;2

Vardy, S. R., Warner, B. G., & Asada, T. (2005). Holocene environmental change in two polygonal peatlands, south-central Nunavut, Canada. *Boreas, 34*(3), 324-334. https://doi.org/10.1111/j.1502-3885.2005.tb01104.x

Vasil'chuk, Y., Budantseva, N., Vasil'chuk, A., Ginzburg, A., & Tokarev, I. (2026). AMS radiocarbon age and stable oxygen and hydrogen isotopes ratio of Holocene ice wedges of the Pur-Taz interfluve. *Radiocarbon, 68*(3), 646-658. https://doi.org/10.1017/RDC.2026.10206

Watmough, S., Gilbert-Parkes, S., Basiliko, N., Lamit, L. J., Lilleskov, E. A., Andersen, R., ... & Zahn, G. (2022). Variation in carbon and nitrogen concentrations among peatland categories at the global scale. PLoS One, 17(11), e0275149. https://doi.org/10.1371/journal.pone.0275149

Webb, E. E., Liljedahl, A. K., Cordeiro, J. A., Loranty, M. M., Witharana, C., & Lichstein, J. W. (2022). Permafrost thaw drives surface water decline across lake-rich regions of the Arctic. *Nature Climate Change, 12*(9), 841-846. https://doi.org/10.1038/s41558-022-01455-w

Wickland, K. P., Jorgenson, M. T., Koch, J. C., Kanevskiy, M., & Striegl, R. G. (2020). Carbon dioxide and methane flux in a dynamic Arctic tundra landscape: Decadal-scale impacts of ice wedge degradation and stabilization. *Geophysical Research Letters, 47*(22), e2020GL089894. https://doi.org/10.1029/2020GL089894

Wolter, J., Lantuit, H., Fritz, M., Macias-Fauria, M., Myers-Smith, I., & Herzschuh, U. (2016). Vegetation composition and shrub extent on the Yukon coast, Canada, are strongly linked to ice-wedge polygon degradation. *Polar Research, 35(*1), 27489. https://doi.org/10.3402/polar.v35.27489

Wolter, J., Lantuit, H., Wetterich, S., Rethemeyer, J., & Fritz, M. (2018). Climatic, geomorphologic and hydrologic perturbations as drivers for mid-to late Holocene development of ice-wedge polygons in the western Canadian Arctic. *Permafrost and Periglacial Processes, 29*(3), 164-181. https://doi.org/10.1002/ppp.1977

Young, D. M., Baird, A. J., Charman, D. J., Evans, C. D., Gallego-Sala, A. V., Gill, P. J., Hughes, P. D. M., Morris, P. J., & Swindles, G. T. (2019). Misinterpreting carbon accumulation rates in records from near-surface peat. *Scientific reports, 9*(1), 17939. https://doi.org/10.1038/s41598-019-53879-8

Young, D. M., Baird, A. J., Gallego-Sala, A. V., & Loisel, J. (2021). A cautionary tale about using the apparent carbon accumulation rate (aCAR) obtained from peat cores. *Scientific Reports*, *11*(1), 9547. https://doi.org/10.1038/s41598-021-88766-8

Zhang, Y., Li, J., Wang, X., Chen, W., Sladen, W., Dyke, L., Dredge, L., Poitevin, J., McLennan, D., Steward, H., Kowalchuk, S., Wu, W., Kershaw, G. P., & Brook, R. K. (2012). Modelling and mapping permafrost at high spatial resolution in Wapusk National Park, Hudson Bay Lowlands. *Canadian Journal of Earth Sciences, 49*(8), 925-937. https://doi.org/10.1139/e2012-031

Zoltai, S. C., & Tarnocai, C. (1975). Perennially frozen peatlands in the western Arctic and Subarctic of Canada. *Canadian Journal of Earth Sciences, 12*(1), 28-43. https://doi.org/10.1139/e75-004

Table 1. Vegetation zone, distance from the coast, peat thickness, total C mass, and basal peat ages (uncalibrated ^{14}C age, calibrated 2-sigma range, and median age) for all study sites. The age calibration was performed using OxCal v4.4 (Bronk Ramsey, 2009) and the IntCal20 calibration curve (Reimer et al., 2020). Long-term peat accumulation rate (PAR; mm a^{-1}) and carbon accumulation rate (LORCA; g C m^{-2} a^{-1}) were calculated by dividing the peat thickness and total C mass by the calibrated median age. Vegetation zones: LAT = low Arctic tundra, ST = subarctic tundra, and NBF = northern boreal forest. *Sites for detailed paleoecological reconstructions.

					AMS Radiocarbon dating								
Site name	Vegetation zone	Distance to coast (km)	Peat thickness (cm)	Total C mass (kg C m^{-2})	Lab ID	Dated material	Depth (cm)	Age (^{14}C yr BP)	2σ range (cal BP)	Median age (cal BP)	PAR (mm a^{-1})	LORCA (g C m^{-2} a^{-1})
Polygonal peatlands												
WAP05B*	LAT	13,5	110	75,0	UOC-26524	Ericaceae leaves, moss stems	109–110	2390 ± 15	2346–2436	2391	0,46	31,4
WAP34A*	ST	46,8	180	94,2	UOC-26523	Bulk peat	179–180	3350 ± 15	3490–3594	3542	0,51	26,6
WAP34B (trough)	ST	46,8	NA	NA	UOC-26532	*Sphagnum* stems, Ericaceae leaves	87–88	645 ± 20	559–594	577	NA	NA
OWL 2.1*	ST	38,9	166	70,4	UOC-26529	Moss stems, Ericaceae leaves	165–166	3460 ± 15	3684–3729	3707	0,45	19,0
IW1*	ST	26,8	105	45,1	UOC-28046	Wood fragments	104–105	3360 ± 20	3492–3684	3588	0,29	12,6
IW4	ST	25,4	94	44,0	UOC-27860	Bulk peat	91–92	3030 ± 30	3083–3346	3215	0,29	13,7
SBF1	ST	43,4	126	67,2	UOC-29266	Wood fragments	125–126	3360 ± 20	3492–3684	3588	0,35	18,7
SKID1	ST	36,6	78	46,7	UOC-29268	Wood fragments	77–78	1580 ± 20	1401–1518	1460	0,53	32,0
Treed peat plateaus												
LSW9	ST	13,8	72	37,1	UOC-30617	Bulk peat	71–72	1840 ± 35	1825–1632	1729	0,42	21,4
LSW10	ST	9,2	66	36,0	UOC-29263	Bulk peat	65–66	365 ± 15	324–489	407	1,62	88,4
SLF5	ST	25,6	76	37,2	UOC-28051	Coniferous needles	75–76	1110 ± 15	957–1058	1008	0,75	36,9
WAP27-1B*	NBF	78,1	251	124,7	UOC-25975	Ericaceae leaves, moss stems, Cyperaceae seeds	250–251	5010 ± 25	5656–5755	5706	0,44	21,9
1994B-TB	NBF	76,9	263	123,5	UOC-30614	Bulk peat	262–263	5190 ± 35	6103–5900	6002	0,44	20,6
Permafrost fens												
PF5	ST	14,7	58	32,3	UOC-28045	*Juncus* seeds	57–58	2090 ± 15	1997–2109	2053	0,28	15,7
Non-permafrost fens												
SSF11	ST	11,4	24	15,0	UOC-27342	Bulk peat	23–24	1560 ± 20	1377–1515	1446	0,17	10,4
PF12	ST	18,6	51	25,8	UOC-27861	Wood fragments	50–51	2160 ± 30	2006–2305	2156	0,24	12,0
LMF6	ST	13,7	38	19,1	UOC-28047	Wood fragments	36–37	1280 ± 15	1177–1276	1227	0,31	15,6
HLG-1	ST	15,2	51	20,6	UOC-29267	Bulk peat	47–48	1270 ± 15	1130–1274	1202	0,42	17,2
SLF4	NBF	76,4	37	21,5	UOC-28050	Bulk peat	36–37	2490 ± 20	2492–2713	2603	0,14	8,2
Coastal fens												

CF7	ST	0,8	27	10,4	UOC-28048	Wood fragments	26–27	120 ± 15	30–259	145	1,86	71,9
CF8	ST	0,9	37	16,4	UOC-28049	Moss stems, seeds	36–37	110 ± 15	33–257	145	2,55	113,3

Table 2. Peat and carbon accumulation rates (PAR; CAR), and median C%, N%, and C/N ratios for the zones identified using CONISS hierarchical clustering. PAR (mm a^{-1}) was calculated by dividing the zone thickness by its duration time. Similarly, CAR (g C m^{-2} a^{-1}) was calculated by dividing the C mass in a zone by the duration time. The duration time of a zone was determined as the difference between the median ages (cal BP) at their upper and lower boundaries, as estimated by the Bacon age–depth models. The periods (cal BP) presented in the table are midpoints between the median ages of the start and end of successive zones, rounded to the nearest 10.

Site	Zone	Depth (cm)	Period (cal BP)	Vegetation	PAR (mm a^{-1})	CAR (g C m^{-2} a^{-1})	C% Median	N% Median	C/N ratio Median
WAP05B	1	109–89	2390–2010	*Tomentypnum nitens*	0,56	32,1	39,8	2,10	19,5
	2a	89–52	2010–1110	Calliergonaceae	0,42	25,1	41,8	2,26	18,0
	2b	52–16	1110–190	Calliergonaceae, *Carex* spp.	0,41	32,3	43,1	2,42	17,9
	3	16–0	190–present	*Dicranum spp.*, Ericaceae	0,67	51,9	43,2	0,94	45,9
IW1	1	105–83	3590–2670	Mosses, *Picea mariana*	0,25	13,0	NA	NA	NA
	2	83–59	2670–2170	*Sph. fuscum, Picea mariana*	0,51	15,8	NA	NA	NA
	3a	59–46	2170–1760	*Picea mariana*	0,34	19,8	NA	NA	NA
	3b	46–6	1760–770	*Sph. fuscum, Picea mariana*	0,42	15,8	NA	NA	NA
	3c	0–6	770–present	Lichens, Ericaceae	0,07	4,6	NA	NA	NA
WAP34A	1a	180–159	3540–3140	*Carex* spp., *Larix laricina*	0,51	33,0	40,9	2,76	14,3
	1b	159–104	3140–1760	*Larix laricina, Picea* spp.	0,40	28,3	43,7	1,77	25,2
	2a	104–66	1760–1460	*Sph. fuscum* type, *V. oxycoccos*	1,31	43,4	42,2	0,45	94,8
	2b	66–23	1460–570	*Sph. fuscum* type, *Picea* spp.	0,49	20,8	43,1	0,52	85,1
	2c	23–0	570–present	*Dicranum* spp., *Sph. lenense*	0,37	19,6	42,7	1,05	41,3
OWL 2.1	1a	166–144	3710–2710	Brown mosses, Cyperaceae	0,23	13,2	37,8	2,36	16,3
	1b	92–144	2710–2200	S. sect. *Acutifolia, V. oxycoccos*	1,04	30,6	42,6	0,67	64,5
	2a	92–26	2200–460	*Sphagnum* spp., *Picea* spp.	0,39	18,9	46,2	1,26	37,0
	2b	26–0	460–present	*Sphagnum lenense*	0,55	22,0	41,7	0,53	78,5
WAP271B	1a	251–194	5710–3780	*Carex* spp., *L. laricina,* Betulaceae	0,30	19,5	44,6	2,36	18,7
	1b	194–161	3780–2610	*Picea* spp., *S.* sect. *Acutifolia*	0,29	18,3	44,8	0,83	55,7
	1c	161–139	2610–1600	*Sph. fuscum, Picea* spp.	0,23	9,7	43,7	0,70	68,2
	2	139–49	1600–780	S. sect. *Cuspidata, V. oxycoccos*	1,11	45,4	44,1	0,70	63,4
	3a	49–5	780–30	*Sph. fuscum, Picea* spp.	0,59	24,9	43,7	0,50	87,8
	3b	5–0	30–present	Lichens, *Rhododendron* sp.	0,62	25,4	44,9	1,06	43,3

Table 3. Summary of peatland characteristics, vegetation succession, and peat and C accumulation rates across the studied paleoreconstruction sites in the low Arctic and subarctic tundra and the northern boreal forest zones. The timing of spruce disappearance at WAP27-1B is in parentheses because the peat plateau is still treed, but spruce needles decreased in the peat profile ~590 cal BP. The shift to shrub tundra vegetation, associated with slow peat accumulation, indicates the timing of permafrost aggradation.

	WAP05	IW1	WAP34	OWL 2.1	WAP27-1B
Vegetation zone	Low Arctic	Subarctic	Subarctic	Subarctic	Northern Boreal
Latitude	58,34	58,29	58,05	57,71	57,61
Ecosystem type	Polygonal peatland	Polygonal peatland	Polygonal peatland	Polygonal peatland	Treed peat plateau
Peatland age (cal BP)	2390	3590	3540	3710	5710
Fen-bog transition (cal BP)	~190	~3210	~2300	~2670	~3590
Decline in peat accumulation rate (cal BP)	Not observed	~1050	~1270	~1530	~760
Spruce disappearance (cal BP)	No spruce	~1330	~780	~890	(~590)
Shift from *Sphagnum* bog to shrub tundra vegetation (cal BP)	No *Sphagnum*	~420	~550	~460	~100–20
PAR range during the LIA (mm a^{-1})	0.2–1.4	0.62–0.63	0.3–0.4	0.1–1.0	0.5–0.7
CAR range during the LIA (g C m^{-2} a^{-1})	22.1–112.4	2.5–7.5	12.3–28.3	6.9–36.2	12.5–29.7